# LIVAS: a 3D multi-wavelength aerosol/cloud database based on CALIPSO and EARLINET

**V. Amiridis[1], E. Marinou[1], A. Tsekeri[1], U. Wandinger[2], A. Schwarz[2], E. Gianna-kaki[3], R. Mamouri[4], P. Kokkalis[1], I. Binietoglou[5], S. Solomos[1], T. Herekakis[1], S. Kazadzis[6], E. Gerasopoulos[6], E. Proestakis[1], D. Balis[7], A. Papayannis[8], C. Kontoes[1], K. Kourtidis[9], N. Papagiannopoulos[10], L. Mona[10], G. Pappalardo[10], O. Le Rille[11] and A. Ansmann[2]**

[1] {Institute for Astronomy, Astrophysics, Space Applications and Remote Sensing, National Observatory of Athens, Athens, 15236, Greece; tel: +302108109196, fax: +302106138343}

[2] {Leibniz Institute for Tropospheric Research (TROPOS), Leipzig, Germany}

[3] {Finnish Meteorological Institute, Kuopio Unit, Finland}

[4] {Cyprus University of Technology, Limassol, Cyprus}

[5] {National Institute of R&D for Optoelectronics, Bucharest, Romania}

[6] {Institute of Environmental Research and Sustainable Development, National Observatory of Athens, Greece}

[7] {Aristotle University of Thessaloniki, Thessaloniki, Greece}

[8] {National Technical University of Athens, Zografou, Greece}

[9] {School of Engineering, Democritus University of Thrace}

[10] {Istituto di Metodologie per l'Analisi Ambientale, Consiglio Nazionale delle Ricerche, Potenza, Italy}

[11] {European Space Agency}

Correspondence to: Vassilis Amiridis (vamoir@noa.gr)

**Abstract**

We present LIVAS, a 3-dimentional multi-wavelength global aerosol and cloud optical database, optimized to be used for future space-based lidar end-to-end simulations of realistic atmospheric scenarios as well as retrieval algorithm testing activities. LIVAS database provides averaged profiles of aerosol optical properties for the potential space-borne laser operating wavelengths of 355, 532, 1064, 1570 and 2050 nm and of cloud optical properties at the wavelength of 532 nm. The global database is based on CALIPSO observations at 532 and 1064 nm and on aerosol-type-dependent backscatter- and extinction-related Ångström exponents, derived from EARLINET ground-based measurements for the UV and scattering calculations for the IR wavelengths, using a combination of input data from AERONET, suitable aerosol models and recent literature. The required spectral conversions are calculated for each of the CALIPSO aerosol types and are applied to CALIPSO backscatter and extinction data correspondingly to the aerosol type retrieved by the CALIPSO aerosol classification scheme. A cloud optical database based on CALIPSO measurements at 532 nm is also provided, neglecting wavelength conversion due to approximately neutral scattering behavior of clouds along the spectral range of LIVAS. Averages of particle linear depolarization ratio profiles at 532 nm are provided as well. Finally, vertical distributions for a set of selected scenes of specific atmospheric phenomena (e.g. dust outbreaks, volcanic eruptions, wild fires, polar stratospheric clouds) are analyzed and spectrally converted so as to be used as case studies for space-borne lidar performance assessments. The final global dataset includes 4-year (01/01/2008 – 31/12/2011) time-averaged CALIPSO data on a uniform grid of 1x1 degree with the original high vertical resolution of CALIPSO in order to ensure realistic simulations of the atmospheric variability in lidar end-to-end simulations.

## 1. Introduction

A general methodology to test the ability of candidate future space-borne remote-sensing instruments to observe atmospheric quantities is the application of their processing algorithms on simulated datasets. The datasets are usually based on the instrument characteristics and a description of the atmospheric state. Especially for active remote sensors as lidars, the vertical dimension should be included in the simulations. Global distributions of such data are available today due to the launch of the Cloud-Aerosol Lidar with Orthogonal Polarization (CALIOP) instrument on board the Cloud-Aerosol Lidar and Infrared Pathfinder Satellite Observations (CALIPSO) mission of NASA/CNES in June 2006 (Winker et al., 2009). Ever since, CALIPSO provides global aerosol and cloud vertical distributions to the scientific community through analysis of CALIOP backscatter observations at the operating wavelengths of 532 and 1064 nm.

The technique of active remote sensing of the atmosphere by lidar has been also chosen for two of the future ESA Earth Explorer Missions, namely the Atmospheric Dynamics Mission Aeolus (ADM-Aeolus, Stoffelen et al., 2005) and the Earth Clouds, Aerosols and Radiation Explorer (EarthCARE, ESA-SP-1279(1); Illingworth et al., 2014), and was further proposed for the Advanced Space Carbon and Climate Observation of Planet Earth (A-SCOPE), one of the candidates for the 7th Earth Explorer mission. Atmospheric Laser Doppler Instrument (ALADIN) on-board ADM-Aeolus and ATmospheric LIDar (ATLID) on-board EarthCARE are two High Spectral Resolution Lidars (HSRLs) operating at 355 nm and detecting the backscatter signal from atmospheric aerosols, clouds and molecules in order to retrieve the horizontal component of the wind vector with Doppler techniques (ALADIN) and the vertical profiles of aerosol and cloud backscatter, extinction and particle depolarization (ATLID). The

instrument design proposed for the A-SCOPE mission is an Integrated Path Differential Absorption (IPDA) lidar, aiming at measuring column-averaged dry-air $CO_2$ mixing ratios with high precision and low bias error, based on SWIR (1570 nm or 2050 nm) laser and detector technologies.

The ESA Reference Atmosphere Model (RMA) currently used for the design and the performance validation of ALADIN and ATLID instruments is derived from airborne lidar measurements performed at 10.6 μm over regions of the Atlantic during a relatively clean atmospheric period (1988-1990, Vaughan et al., 1998). This RMA consists of five statistical aerosol backscatter profiles organized by percentiles and one molecular profile with a resolution of 0.5 km from 0 to 16 km altitude. ESA RMA provides also the optical properties of various clouds and the albedos for different surface types (sea/land/ice).

Due to its spatial restrictions, the current ESA RMA is not representative for global simulations. The correct performance assessment of current and future ESA lidar instruments requires the development of a refined aerosol and cloud optical database with high spatial resolution for the Planetary Boundary Layer (PBL), the free troposphere (FT) and the stratosphere. An appropriate RMA should be representative of both statistical atmospheric information (i.e. per atmospheric region, climate zone and season) and deterministic information (i.e. extended atmospheric scenes with, e.g., Saharan dust events, biomass-burning aerosol events, volcanic eruption events, polar stratospheric cloud events, convective cloud events). Moreover, the RMA should include multi-wavelength parameters so as to cover the spectral domain of future HSRL and IPDA lidar missions, specifically the three harmonic operating wavelengths of Nd:YAG lasers (355, 532 and 1064 nm) and typical wavelengths of future IPDA lidars in the SWIR spectral domain (1.57 and 2.05 μm).

Over the recent years, the European Aerosol Research Lidar Network (EARLINET, http://www.earlinet.org/, Pappalardo et al., 2014) and the Aerosol Robotic Network (AERONET, http://aeronet.gsfc.nasa.gov/, Holben et al., 1998) ground-based lidar and sunphotometer networks, respectively, along with the CALIPSO backscatter lidar mission have provided new resources that can be used for the elaboration of such a multi-wavelength database for typical laser operating wavelengths. Additionally, several airborne and ground-based field experiments involving in-situ instrumentation together with HSRL and multi-wavelength Raman lidar systems have been performed over the last twenty years and can be very useful for the consolidation of such a RMA. In this paper we present the "LIdar climatology of Vertical Aerosol Structure for space-based lidar simulation studies" (LIVAS) which is a RMA aiming to provide profiles of aerosol and cloud optical properties on a global scale, that can be used for the simulation of realistic atmospheric scenarios in current and future lidar end-to-end simulations and retrieval algorithm testing activities. For HSRL and IPDA lidar applications, LIVAS addresses the wavelength dependency of aerosol optical properties for the following laser operating wavelengths: 355 nm, 532 nm, 1064 nm, 1.57 μm and 2.05 μm. Moreover, LIVAS includes regional and seasonal statistics of aerosol and cloud extensive and intensive optical properties in terms of backscatter coefficient, extinction coefficient and particle linear depolarization ratio. Furthermore, vertical profiles of extensive and intensive optical properties referring to specific atmospheric scenes for a set of selected scenarios are provided (i.e. Saharan dust, smoke from biomass burning, ash from volcano eruptions, polar stratospheric clouds). The data used for the development of LIVAS are presented in Section 2 while the methodologies followed are given in Section 3. LIVAS product and its validation are presented in Section 4, and the paper closes with our conclusions in Section 5.

## 2. Data

### 2.1. The CALIPSO Level 2 product

CALIOP, the principal instrument on board the CALIPSO satellite, part of the NASA A-Train, is a standard dual-wavelength (532 and 1064 nm) backscatter lidar, operating a polarization channel at 532 nm (Winker et al., 2009). CALIOP has been acquiring high-resolution profiles of the attenuated backscatter of aerosols and clouds at 532 and 1064 nm along with polarized backscatter in the visible channel since 2006 (Winker et al., 2009). The horizontal resolution of CALIPSO is 1/3 km while the vertical resolution is 30 m in the tropospheric region (between the surface and 20 km) and 180 m in the stratospheric region (between 20 and 30 km). This data is distributed as part of CALIPSO Level 1 products.

After calibration and range correction, cloud and aerosol layers are identified and aerosol backscatter and extinction at 532 and 1064 nm are retrieved as part of the Level 2 product. The product is produced by the application of a succession of algorithms that are described in detail in a special issue of the Journal of Atmospheric and Oceanic Technology (e.g., Winker et al., 2009). In brief, the CALIOP Level 2 retrieval scheme is composed of feature detection and subtyping algorithms (modules that classify features), and an extinction retrieval algorithm that estimates the aerosol backscatter and extinction coefficient profile and total column aerosol optical depth (AOD) using an assumed lidar ratio (LR) for each detected aerosol layer (the lidar ratio is calculated only in cases when clear air is available both above and below a layer (Young and Vaughan, 2009)) . The final CALIPSO Level 2 product includes the vertical location of layers (Vaughan et al., 2009), the discrimination of aerosol layers from clouds (Liu et al., 2009), the categorization of the aerosol layers in six subtypes (dust, marine, smoke, polluted dust, polluted continental, and clean continental; Omar et al., 2009),

and AOD estimations for each layer detected (Young and Vaughan, 2009). Due to CALIOP's sensitivity to polarization at 532 nm, the depolarization arising from scattering from non-spherical dust particles serves as an independent means of discrimination between dust and other aerosol species. In this study we use the Version 3 of the Level 2 product (Young and Vaughan, 2009).

### 2.2. The EARLINET product

EARLINET (http://www.earlinet.org) has been operating since 2000 aiming to establish a quantitative and comprehensive database for the aerosol vertical, spatial and temporal distribution of aerosols on the European continental scale (Pappalardo et al., 2014). To date, EARLINET includes 27 stations in 16 countries performing lidar observations on a regular schedule of one daytime measurement per week around noon and two nighttime measurements per week with low background light in order to perform Raman extinction measurements (see Table 1 in Pappalardo et al., 2014). The first volumes of the EARLINET database have been published in biannual volumes at the World Data Center for Climate (The EARLINET publishing group 2000-2010, 2014 a, b). In addition to the routine measurements, further observations are devoted to monitor special events such as Saharan dust outbreaks, forest fires and volcano eruptions (The EARLINET publishing group 2000-2010, 2014 d, e). Moreover, since 14 June 2006 EARLINET has carried out collocated measurements with CALIPSO during nearby overpasses, following a strategy defined on the basis of the ground-track data analysis provided by NASA (Pappalardo et al., 2010; The EARLINET publishing group 2000-2010, 2014c).

EARLINET operation is coordinated such as to ensure instrument standardization and consistent retrievals within the network. This harmonization is achieved through the application of a rigorous quality-assurance program addressing both instrument per-

formance (Matthias et al., 2004; Freudenthaler et al., 2010) and evaluation of the algorithms (Böckmann et al., 2004; Pappalardo et al., 2004).

The 14-year EARLINET database contains a large dataset of the aerosol lidar ratio retrieved from simultaneous and independent lidar measurements of aerosol extinction and backscatter coefficients. Moreover, this multi-wavelength database facilitates the retrieval of extinction and backscatter spectral dependence for different aerosol types after a proper layer identification and characterization. Such intensive properties are of fundamental importance for the estimation of aerosol extinction from pure backscatter lidar measurements such as conducted by CALIPSO (i.e. the lidar ratio), as well as for the spectral conversions between laser wavelengths.

### 2.3. The AERONET product

AERONET (http://aeronet.gsfc.nasa.gov/) is a global sunphotometric network with more than 250 stations, employing the CIMEL CE318 photometer as the standard instrument (Holben et al., 1998). In AERONET, the calibration is centralized and should be performed every 12 months, thus the instrument must be sent to specific sites (in United States or Europe) for calibration and maintenance. AERONET measurement schedule includes direct sun measurements at several wavelengths of the solar spectrum (at 380, 440, 500, 675, 870, 1020 and 1640 nm depending on the instrument type) as well as diffuse sky radiances at 440, 675, 870 and 1020 nm. Direct sun measurements are used to retrieve the AOD at the measured wavelengths, the Ångström exponent at 440/870 nm, and fine and coarse mode optical depth at 500 nm (Holben et al, 2001; O'Neill, 2003). Direct sun and sky radiance measurements permit the retrieval of the size distribution, the complex refractive index, and the Single-Scattering Albedo (SSA) (Dubovik and King, 2000; Dubovik et al, 2000, Dubovik et al. 2006).

## 3. Methods

In this section we describe the methods developed for the derivation of the multi-wavelength LIVAS database. LIVAS has developed based on CALIPSO observations at 532 and 1064 nm and includes converted CALIPSO extinction and backscatter product from 532 nm to 355, 1570 and 2050 nm (LIVAS wavelengths). For the spectral conversion from CALIPSO 532 nm to the LIVAS wavelengths, we use aerosol-type-dependent backscatter- and extinction-related Ångström exponents, as these are derived from ground-based measurements or suitable optical models. Specifically, for the conversions applied in LIVAS, the spectral dependence of the extinction and backscatter is considered to follow the well-known Ångström exponential law as follows:

$$x_{par}(\lambda_2) = x_{par}(\lambda_1)\left(\frac{\lambda_1}{\lambda_2}\right)^{\dot{A}_{\lambda_1/\lambda_2}} \qquad \text{(Eq. 1)}$$

where $x_{par}(\lambda_2)$ is the converted extinction or backscatter at $\lambda_2$ (either 355, 1570 or 2050 nm), $\dot{A}_{\lambda_1/\lambda_2}$ is the BAE or EAE and $x_{par}(\lambda_1)$ is the extinction or backscatter product of CALIPSO at $\lambda_1$=532 nm. In the following, instead of extinction-related Ångström exponents and backscatter-related Ångström exponents we use the terms EAE and BAE respectively to describe the spectral dependence of the extinction and backscatter.

An overview of the data and methods followed for the derivation of the aerosol-type-dependent BAE and EAE is schematically illustrated in Figure 1, while the aerosol model developed for LIVAS is detailed, discussed and evaluated in paragraph 3.1. The methodology for the spectral conversion of the CALIPSO Level 2 product is demonstrated through an example presented in paragraph 3.2. The section closes with the description of the processing chain followed for quality filtering and averaging the CALIPSO observations, given in paragraph 3.3.

### 3.1. Aerosol model for the derivation of spectral conversion factors

For the derivation of the BAE and EAE we constructed the LIVAS aerosol model with typical microphysical and optical properties for each CALIPSO aerosol type. Different methods and datasets are utilized for the UV and IR spectral regions, as described in detail below. The microphysical and optical properties of each CALIPSO type in the model are provided in Tables 1 and 2.

BAE and EAE for the 532 to 355 nm conversion are mainly derived from multi-wavelength EARLINET measurements of the extinction and backscatter coefficients. EARLINET measurements cannot be used for the IR conversion since the ground-based lidars of the network are spectrally limited between 355 and 1064 nm. Thus, for converting the CALIPSO backscatter and extinction products from 532 nm to 1570 and 2050 nm, we first defined the typical size distributions and refractive indexes of the six aerosol subtypes used by CALIPSO (i.e. dust, polluted dust, smoke, marine, clean continental and polluted continental), and then we calculated the respective BAE and EAE utilizing well-known scattering codes like the Mie code for spherical particles (Mie, 1908; Van de Hulst, 1957), as well as the T-matrix code (Mishchenko et al., 2002) and the geometric-optics-integral-equation technique (Yang and Liou, 1996) for non-spherical particles.

The construction of representative size distributions and refractive indexes corresponding to the CALIPSO aerosol types is not a straight-forward task. Aerosol classification for CALIPSO is based on a threshold algorithm that takes into account the layer-integrated attenuated backscatter coefficient and an approximate particulate depolarization ratio as well as the surface type (either land or ocean; Omar et al., 2009). However, these properties do not provide all the information needed for unambiguously classifying the aerosol type and, as a result, misclassifications occur frequently

(e.g. Burton et al., 2013). Since for LIVAS model we need to calculate BAE and EAE assuming that the CALIPSO aerosol types are representative of the aerosols observed, any inconsistencies in the CALIPSO classification scheme introduce inaccuracies in our results. The CALIPSO aerosol model on the other hand, is introduced due to the need for a-priori knowledge of the LR, and it consists of typical size distributions and refractive indexes for each type that are retrieved by clustering AERONET measurements in respective categories/aerosol types, as described in Omar et al. (2005; 2009). Although the proposed classification is assumed to correspond to the independently derived CALIPSO aerosol types, this is not true for all cases, mainly due to the different nature of AERONET sunphotometer measurements versus CALIPSO lidar measurements used for the categorization. This is the reason we do not use it for the calculation of LIVAS BAE and EAE.

In LIVAS, we initialize a number of different approaches to construct a representative aerosol model for CALIPSO and we evaluate it using the ground-based lidar measurements of EARLINET. We emphasize that in contrast to the sunphotometer-only method used for the CALIPSO aerosol model, the lidar-related methodology presented here is considered more appropriate for the CALIPSO aerosol classification scheme. This is because EARLINET performs direct ground-based lidar measurements of the backscatter coefficient in contrast to the CIMEL sunphotometer which is incapable of providing measurements at the scattering angle of $180^{\circ}$.

Summarizing, the LIVAS aerosol model contains the measured BAE and EAE from EARLINET data for the UV-VIS and the calculated BAE and EAE for the VIS-IR spectral range. For the latter we employed characteristic size distributions and refractive indexes from AERONET data classified into the respective aerosol types using different approaches. The results are validated against EARLINET measurements.

Moreover, for aerosol types that are not probed by either EARLINET or AERONET (e.g. marine), we utilize typical properties from the Optical Properties of Aerosols and Clouds (OPAC) model (Hess et al., 1998) or other aerosol models from the literature. An elaborated description of our methodology for the UV-VIS and VIS-IR spectral regions is given in paragraphs 3.1.1 and 3.1.2, respectively.

### 3.1.1. BAE and EAE in UV-VIS spectral region

For the conversion of CALIPSO aerosol backscatter and extinction from 532 to 355 nm, the aerosol-type-dependent BAE and EAE were derived from the EARLINET database. Specifically, we used the database developed within the project "EARLINET's Space-borne-related Activity during the CALIPSO mission" (ESA-CALIPSO, Wandinger et al., 2011). ESA-CALIPSO was an ESA-funded study aimed to establish an aerosol database from the classification of EARLINET observations performed during nearby CALIPSO overpasses with respect to the aerosol type. The methodology followed and the objectives of ESA-CALIPSO are described in Wandinger et al. (2011). In brief, during ESA-CALIPSO a large number of EARLINET observations was utilized to develop an aerosol classification scheme over Europe and to determine the respective type-dependent BAE and EAE and other intensive properties. Each EARLINET measurement was inspected regarding quality (e.g., noise level) and the occurrence of distinct aerosol layers. For each selected layer, an air-mass transport simulation was performed to determine its origin, transport path, and age. Additional modeling tools and satellite products (e.g., fire maps) were implemented to cross-check the sources and to assign an aerosol type for each layer (Wandinger et al., 2011).

For the derivation of the UV/VIS (355 from 532 nm) BAE and EAE in LIVAS, we used more than 500 aerosol layers recorded in the ESA-CALIPSO database and pro-

vided by four high-performance EARLINET stations, namely the stations of Athens, Leipzig, Potenza and Thessaloniki. The final BAE and EAE were calculated by averaging the measurements collected for each aerosol type. These are presented in the left column of Table 3 for backscatter (bsc) and extinction (ext).

The EARLINET measurements included in ESA-CALIPSO regarding clean marine, clean continental and stratospheric aerosol particles are limited for a reliable statistical analysis. The calculation of BAE is possible, but for EAE this is not the case (mainly due to Raman lidar constraints regarding the overlap that prohibits extinction retrievals for lower marine atmospheric layers and regarding inadequate Raman returns from the stratosphere). For the aforementioned types, aerosol models provided in the literature are used in order to calculate the EAE. Specifically, we used the maritime model introduced in Sayer et al. (2012) for clean marine aerosols, the OPAC model for clean continental aerosols and the stratospheric model of Wandinger et al. (1995) and Deshler et al. (1993) for stratospheric aerosols. From these models, typical size distributions and refractive indexes were retrieved and BAE and EAE were calculated via the application of the Mie theory (Mie, 1908; Van de Hulst, 1957). The results are given in Table 3 (left column).

### 3.1.2. Conversion factors in VIS-IR spectral region

ESA-CALIPSO is mainly limited to the VIS-UV spectral region. For the VIS-IR conversions in LIVAS, we used typical size distributions and refractive indexes for each aerosol type derived from AERONET data or models, i.e. OPAC or other aerosol models in the literature. Scattering simulations were then applied for each aerosol type for the complete spectral range of LIVAS interest (i.e. 355, 532, 1064, 1570, 2050 nm). The criterion for selecting between different approaches for each aerosol type was the consistency of the calculations in the UV-VIS spectral region with the ESA-

CALIPSO measurements, which were the reference for any conversion made in LIVAS. More specifically, we checked the consistency of our calculations with ESA-CALIPSO for the 532-to-355-nm EAE and the 532-to-355-nm, 1064-to-355-nm and 1064-to-532-nm BAE. Based on its consistency with ESA-CALIPSO, the approach selected for the derivation of the typical microphysical and optical properties of each aerosol type is described in the following:

AERONET-Omar: AERONET data were categorized with respect to the CALIPSO aerosol types based on the classification method introduced by Omar et al. (2005; 2009), utilized for the construction of the CALIPSO aerosol model as described above. The difference in our approach for the LIVAS aerosol model is that for each aerosol type a consistency check with the ESA-CALIPSO data was first performed: each AERONET measurement was categorized under a specific aerosol type and the Ångström exponent at 355/532 nm and the lidar ratios at 355 and 532 nm were computed (using the phase function and the SSA provided by AERONET). Then, we rejected the cases for which the aforementioned calculated optical properties were not within the range of the typical ESA-CALIPSO values for the respective aerosol type. From the constrained dataset, the average size distribution and refractive index were produced for each aerosol type and subsequently used as input in scattering calculations to produce the spectral conversion factors in the UV-IR spectral range. The method was expected to derive consistent microphysics with ESA-CALIPSO at the UV-VIS range and thus the results for the VIS-IR spectral range would be consistent.

For the scattering calculations the well-known Mie code (Mie, 1908; Van de Hulst, 1957) was applied for all the aerosol types except the non-spherical particles of dust and polluted dust, where the T-matrix code and the geometric-optics-integral-equation technique were utilized instead. More specifically, for the non-spherical scattering

calculations we employed the code of Dubovik et al. (2006), which utilizes the T-matrix method for particles of size parameter ($\frac{2\times\pi\times radius}{wavelength}$) smaller than 20-30 and the geometric-optics-integral-equation technique for larger particles, with size parameter up to ~625. The non-spherical particles are considered as mixtures of spheroids with aspect ratios defined by an aspect-ratio distribution, and pre-computed look-up tables are utilized, allowing fast calculations. We considered that the non-spherical particles of dust and polluted dust over their entire size range have the same aspect ratio distribution as the one provide for dust in Dubovik et al. (2006), which was shown to reproduce successfully the laboratory measurements of mineral dust scattering properties by Volten et al. (2001).

AERONET-CALIPSO: AERONET and CALIPSO collocated and synchronized measurements were collected, following the collocation method introduced in Schuster et al. (2012). More specifically, the spatial collocation required the CALIPSO overpass to be closer than 80 km from the AERONET station and the measurements to take place with maximum 30 min difference. From the collocated measurements, only those with a single CALIPSO aerosol subtype in the atmospheric column were considered. The AERONET data for these cases were subsequently classified based on the aerosol type provided by the collocated CALIPSO measurements. Scattering calculations were applied to each of the AERONET size distributions and refractive indexes of the collected cases taking into account the spherical and non-spherical part of the mixture, as this was provided by AERONET for each case.

It should be highlighted here that for this method there was no distinction between spherical and non-spherical aerosol types, instead all types were considered to contain both spherical and non-spherical particles, in accordance with the AERONET product. The calculations for the spherical part were performed with the Mie code and for

the non-spherical part with the Dubovik et al. (2006) code, following the methodology described above. For each type, all the collocated cases were averaged and from those measurements we derived the average values of BAE and EAE.

The dataset was not constrained with ESA-CALIPSO as in the AERONET-Omar approach for the UV/VIS wavelengths. This was due to the fact that the specific approach aimed to deliver typical BAE and EAE for the aerosol types classified by the CALIPSO classification scheme itself, thus no correspondence to the nature of the atmospheric aerosol loads was required.

OPAC: A typical size distribution and refractive index were extracted from the OPAC dataset for the clean continental type, considering typical ambient conditions of 70% relative humidity. We derived the conversion factors by performing scattering calculations with the Mie code. Since for the clean continental aerosol there is little to no information from AERONET and EARLINET we had to rely on models to derive LIVAS BAE and EAE.

Approaches taken from the literature: The studies of Wandinger et al. (1995) and Deshler et al. (1993) provide a range of typical size distributions and refractive indexes for the stratospheric aerosol, while the maritime model of Sayer et al. (2012) provides a typical size distribution and refractive index for marine aerosol. We derived BAE and EAE by performing scattering calculations with the Mie code.

### 3.1.3. LIVAS aerosol model evaluation against ESA-CALIPSO database

As already mentioned, the aim of the LIVAS aerosol model is to reproduce spectral conversion factors that are consistent with ESA-CALIPSO, a reference database of measured lidar-related aerosol properties, especially regarding the backscatter coefficient, the lidar ratio, and the spectral dependence of the backscatter. While the UV-VIS BAE and EAE were derived directly from the ESA-CALIPSO database, the VIS-

IR BAE and EAE were calculated using the datasets and methods described in section 3.1.2. To ensure consistency of our calculations with measured data, for each aerosol type we selected the VIS-IR methodology that provided compatible results with the ESA-CALIPSO for the UV-VIS BAE and EAE. In this way we ensure the best possible consistency of BAE and EAE for the entire spectral range.

Our final results are presented and discussed herein: Figure 2 shows the calculated BAE and EAE using all the approaches described above and their comparison with ESA-CALIPSO at UV-VIS. The selected approach for each aerosol type is denoted in Figure 2 with large size symbols. Starting from the AERONET-Omar approach, we found that it performed better when compared to ESA-CALIPSO for the polluted continental type, resulting in a very good agreement for the EAE and best performance regarding the BAE. For the other types this approach reproduced well the EAE but the BAE could not be reproduced such as to fit the ESA-CALIPSO acceptable range of values. Dust and polluted dust aerosols are most likely classified correctly by CALIPSO due to its polarization sensitivity (e.g. Burton et al., 2013; Amiridis et al., 2013). For this reason, we chose the AERONET-CALIPSO approach for the calculation of their BAE and EAE. The approach showed a relatively better agreement with ESA-CALIPSO compared to the AERONET-Omar approach, especially for the BAE, maybe due to better filtering of the AERONET data used in the calculations for the AERONET-CALIPSO approach (Figure 2). Overall though, we believe that the discrepancies in backscatter spectral dependence observed for most of the aerosol types are most likely due to the fact that AERONET lacks the capability to directly measure in the backscattering direction. Comparisons found in the literature between Raman-lidar-measured and photometer-retrieved lidar ratio, support this argument (e.g. Mueller et al., 2007).

Moreover, it should be noted though that the evaluation of the retrieved values with ESA-CALIPSO for polluted dust is only indicatory. This is because CALIPSO assumes the same properties for any kind of dust mixture (e.g. dust-smoke, dust-marine), while ESA-CALIPSO shows that the optical properties are highly variable for different dust mixtures. Specifically, ESA-CALIPSO provides intensive properties for mixtures of dust with polluted continental, smoke and marine aerosol separately and what we used here in order to compare with CALIPSO is an average of these properties.

For smoke aerosols the AERONET-CALIPSO approach showed similar results as AERONET-Omar, performing well for EAE, but failing to reproduce the ESA-CALIPSO BAE (Figure 2). For this aerosol type we chose to include in the LIVAS model the calculated BAE and EAE from the AERONET-CALIPSO approach. This decision was based on the fact that the classification of smoke by CALIPSO is the most uncertain compared to the other aerosol types, as reported by Burton et al. (2013). The authors of this study report a percentage agreement of 13% for smoke classification when comparing with airborne HSRL classification results. Smoke misclassification was also found to be the reason of the discrepancies between CALIPSO and AERONET reported in Schuster et al. (2012) in terms of AOD measurements. These findings indicate that the CALIPSO smoke classification may not correspond to real smoke presence. For this reason, it may not be comparable with real smoke detections by EARLINET used for ESA-CALIPSO classification model, which is based on source-receptor analysis based on model simulations of air mass advection over the stations, together with the aerosol optical properties measured by the lidar that are used for aerosol characterization. Thus, for the smoke type we avoided to use the ESA-CALIPSO smoke statistics.

For clean marine and clean continental aerosol, the ESA-CALIPSO database does not contain an adequate number of measurements to provide statistically significant averages. Thus, for clean marine we used the size distribution and refractive index provided in the maritime model of Sayer et al. (2012) and for clean continental we used the ones provided in the OPAC database. Note that the size distribution and refractive index for clean continental aerosol from OPAC database were considered at ambient conditions of 70% relative humidity.

Finally, for the stratospheric aerosol type we used the model introduced in Deshler et al. (1993) and Wandinger et al. (1995). BAE and EAE found to be in good agreement with ESA-CALIPSO values (not shown in Figure 2).

The final aerosol-type-dependent VIS-IR BAE and EAE used in LIVAS are presented in the right panel of Table 3 for extinction (ext) and backscatter (bsc). Overall, as seen in Figure 2, the LIVAS aerosol model in the VIS-IR is compatible with ESA-CALIPSO in the VIS-UV spectral region regarding EAE. However, the agreement with regard to the VIS-UV BAE is not that satisfactory. For the extinction and backscatter-related conversion factors in the IR, one point of concern is the extrapolation of the refractive index at the longer wavelengths, since this information is not provided from AERONET.

### 3.1.4. Comparison of LIVAS and CALIPSO aerosol models

The microphysical properties used for calculating the VIS-IR BAE and EAE are compared in this section with the ones in the CALIPSO aerosol model (Omar et al. 2005; 2009). Figure 3 shows the comparison of LIVAS versus CALIPSO size distributions for each aerosol type, while Figure 4, 5 and 6 show the spectral dependence of the complex refractive index and the SSA, respectively, at LIVAS wavelengths for the two models. Figure 7 shows BAE and EAE at 355/532 nm, the lidar ratio at 532 nm

and the effective radius for the LIVAS and CALIPSO aerosol models, compared with the ones provided in the ESA-CALIPSO database. The values of the lidar ratio at 532 nm, the SSA at 532 nm and the effective radius for the two models are also provided in Table 2.

In Figure 3 the best agreement between the LIVAS and the CALIPSO model size distributions is found for the polluted continental type. For smoke particles the CALIPSO model considers the same volume for fine and coarse particles, whereas the LIVAS model presents a domination of the fine mode. The latter agrees well with the averaged size distribution of smoke type provided in Dubovik et al. (2002) AERONET eight-year climatology and is considered more typical as it is supported by other studies as well as (Reid et al., 2005; Eck et al., 1999; 2003). For dust type the LIVAS size distribution has fewer fine particles than the CALIPSO model, in agreement with the AERONET climatology of Dubovik et al. (2002) and findings of experimental campaigns dedicated to mineral dust characterization (e.g. McConnell et al., 2008; Weinzierl et al., 2009; Müller et al., 2011; Toledano et al., 2011). For the polluted dust type both models seem to fall within the range of the large variability reported in the literature for dusty mixtures (Eck et al., 1999; Jung et al., 2010). The more pronounced fine mode in the LIVAS model resembles the size distributions of dust and pollution mixtures (Kim et al., 2007). However, an extensive discussion on the polluted dust type is avoided here since there is no clear definition of the non-dust components for this type in the CALIPSO model. LIVAS size distribution for clean marine type is based on the maritime model of Sayer et al. (2012). Similar size distributions for marine particles are provided in other studies as well (e.g. Dubovik et al., 2002; Smirnov et al., 2002). The largest disagreement is seen for the clean continental type. We believe that the pronounced fine mode in the LIVAS size distribution from

OPAC is due to the hygroscopic growth of the hydrophilic fine particles in ambient relative humidity of 70%. However, the clean continental type in global CALIPSO records has a contribution of the order of 2%, making this type of less importance for LIVAS database. For the aerosol model though, a better definition of the aerosol components of this type should be considered.

Regarding the differences on the refractive index assumed by LIVAS and CALIPSO aerosol models, these are presented in Figures 4 and 5, respectively for the reader's reference. We also present a comparison of the LIVAS and CALIPSO SSA in Figure 6. The comparison shows an overall disagreement in the SSA between the two aerosol models. We should note here that Omar et al. (2009) provide the refractive index values at 532 and 1064 nm and we used linear extrapolation to construct the CALIPSO aerosol model for all the wavelengths of LIVAS (see Figures 4 and 5). Despite the disagreement of the SSA values, their spectral slope is similar for all the types (except the clean continental aerosol) for both models. Even more so, for polluted continental, dust, smoke and clean marine particles the spectral slope of the SSA agrees relatively well with the corresponding ones provided in Dubovik et al., (2002) climatology. More specifically, for the dust type the spectral slope of the SSA for both models is flatter but it closely resembles the one presented in Dubovik et al. (2002), as well as in other studies (Müller et al., 2011; Toledano et al., 2011). For smoke, the absorption has to do mainly with the black carbon content and can greatly vary (Eck et al., 2003). The spectral dependence and range of SSA values in LIVAS model are similar with the values provided in Dubovik et al. (2002) climatology and references therein, whereas the CALIPSO model presents lower values, which although agree with other studies (e.g. Eck et al., 1998; 2003). The polluted dust SSA spectral dependence is similar for both models, but different than of dust mixtures with smoke and pollution

presented in the literature (e.g. Jung et al., 2010; Holler et al., 2003). Finally, the clean marine SSA for both models agrees very well with other studies in the literature (e.g. Dubovik et al, 2002; Hasekamp et al., 2011).

In Figure 7, a final comparison between ESA-CALIPSO, LIVAS and CALIPSO aerosol models is given in terms of BAE and EAE, lidar ratio at 532 nm and effective radius. We need to highlight here that our focus in evaluating LIVAS model is the BAE and EAE consistency with the ESA-CALIPSO measurements. The lidar ratio and effective radius are not used in generating LIVAS database and are only provided here for reasons of completeness. More work is needed to develop an aerosol model oriented for space-borne lidar applications. BAE and EAE at 355/532 nm for the CALIPSO aerosol model are not provided by Omar et al. (2009) and instead they were calculated using the size distribution and refractive index of the CALIPSO model. For the scattering calculations we used the Mie code for the types with spherical particles and the Dubovik software for the non-spherical particles of dust and polluted dust types. The methodology was the same as the one described for the AERONET-Omar approach in Section 3.1.2. The lidar ratio at 532 nm was taken directly from what is reported in Omar et al. (2009), while due to the fact that the effective radius is not given in this work, it was calculated from the size distribution for each type therein. The maximum deviation was found for BAE, especially for the dust type (Figure 7 upper-right). It is a possibility that one of the reasons of this discrepancy is the lower effective radius produced from the large fine-mode contribution in the size distribution assumed in Omar et al. (2009). For polluted continental aerosol we got a relatively good agreement for the LIVAS and CALIPSO models, in accordance with the ESA-CALIPSO data as well. For smoke aerosol the agreement was also good for both models, but both were not consistent with the ESA-CALIPSO for the backscatter con-

version. For clean marine and clean continental aerosol the LIVAS model agreed well with ESA-CALIPSO, but this was not the case for the CALIPSO model. Overall, we found that the LIVAS and CALIPSO aerosol models agreed only for the polluted continental aerosols, whereas for the rest of the aerosol types the LIVAS model was closer to the ESA-CALIPSO measured values than the CALIPSO model.

### 3.1.5. Spectral conversions for other LIVAS products

Depolarization spectral conversions were not applied in LIVAS since multi-wavelength depolarization measurements are rare and available only during experimental campaigns (Freudenthaler et al., 2009; Groß et al., 2011a, b), thus the dataset was not considered statistically significant. A single-wavelength depolarization database is provided in LIVAS using CALIPSO Level 2 particle depolarization ratio averages at 532 nm.

Furthermore, a global cloud database is given based on CALIPSO observations at 532 nm. With respect to clouds, the wavelength conversion is most probably of minor importance due to approximately neutral scattering behavior along the range of LIVAS wavelengths.

In addition, a database for the stratospheric features detected by CALIPSO is provided, separated to cloud and aerosol features. Specifically, the stratospheric features detected by CALIPSO were separated in polar stratospheric clouds and stratospheric aerosols using the temperature threshold technique proposed by Pitts et al. (2009). In brief, we classified stratospheric features as Polar Stratospheric Clouds (PSCs) for temperature lower than 198 K, while features of higher temperatures were classified as stratospheric aerosols. The separation was applied only for stratospheric features at latitudes greater than 54° N and less than -54°S, while for the latitudes in between, the stratospheric features were considered as aerosols. This classification is not consid-

ered reliable enough and has been included in LIVAS in order to provide only a rough estimate of the stratospheric aerosol loads detected by CALIPSO. More efforts will be needed in the future for achieving a trustworthy separation of different stratospheric features. As proposed by Pitts et al. (2009), the utilization of L1 CALIPSO product in synergy with L2 may provide a more reliable discrimination.

Finally, a set of selected scenes of specific atmospheric phenomena (e.g. dust outbreaks, volcanic eruptions, wild fires, polar stratospheric clouds) was produced. BAE and EAE for the selected scenes were delivered after thorough investigation of each case study, based on CALIPSO-collocated ground-based measurements that are reported to the literature. Whenever this was not possible (as for the IR conversion), the LIVAS BAE and EAE were used.

### 3.2. Example for the spectral conversion of single CALIPSO profiles

The obtained aerosol-type-dependent BAE and EAE for VIS-to-UV and VIS-to-IR were applied to the CALIPSO Level 2 product at 532 nm for the respective aerosol layer type inferred by the CALIPSO aerosol classification scheme. An example of the conversion from 532 to 355 nm is presented in Figure 8. Each CALIPSO layer in the profile example was converted from 532 to 355 nm using the LIVAS EAE at 532/355, depending on the aerosol type retrieved by the CALIPSO aerosol classification scheme for the layer. In the example presented in Figure 8, LIVAS EAE for clean marine (0.78), dust (0.55) and polluted continental (1.24) types were applied to the CALIPSO extinction coefficient at 532 nm, based on the Ångström exponential law described in Equation 1.

### 3.3. CALIPSO quality filtering and averaging processing chain

For the production of the final LIVAS products, we used the methodology developed by the CALIPSO team for the Level 3 aerosol product, as described in Winker et al. (2013). Our algorithm was tested for reproducing the CALIPSO Level 3 product, which is an aggregation onto a global 2x5 degree latitude-longitude grid. After the positive evaluation of the averaging procedure (not shown here), we applied it on Level 2 CALIPSO profiles at 532 and 1064 nm but also on the corresponding LIVAS spectrally converted profiles at 355, 1570 and 2050 nm in order to derive 1x1 degree latitude-longitude averaged vertical distributions. The vertical resolution of the LIVAS product is identical to CALIPSO Level 3, namely 60 m in the tropospheric region between the surface and 20 km and 180 m in the stratospheric region between 20 and 30 km.

As input to the averaging algorithm, we used the Version 3 CALIOP Level 2 aerosol profile product, which is quality screened prior to averaging, to eliminate samples and layers that were detected or classified with very low confidence, or that contained untrustworthy extinction retrievals. In brief, the filters concerned the Cloud-Aerosol Discrimination (CAD) score, Extinction Quality Control (QC) flag, aerosol extinction uncertainty, isolated 80 km layer, misclassified cirrus, undetected surface attached aerosol low bias, large negative near-surface extinction, surface contamination beneath surface-attached opaque layer, removal of samples below opaque cloud and aerosol layers. Detailed explanation of the methodology followed for the production of the Level 3 product and respective filtering and flags, is provided in the Appendix of Winker et al. (2013). For the particle linear depolarization, an extra filter was applied in LIVAS in order to average this parameter for the same samples collected for the extinction. For that, we averaged only particle linear depolarization CALIPSO re-

trievals for which the extinction uncertainty is less than 99.9 $km^{-1}$, so as to maintain the same measurement sampling. For the quality screening of cloud and stratospheric feature profiles a similar methodology was followed.

In the CALIPSO Level 3 product, four types of products were generated each month, depending on sky condition and temporal coverage, and were separated into day/night segments. In LIVAS, only the "combined" product was used (Winker et al. 2014) in order to achieve better quality of the aerosol dataset regarding cloud discrimination and measurement accuracy. Moreover, beyond the mean extinction profiles for the total aerosol load, LIVAS provides mean extinction profiles at 532 nm for each of the six aerosol types in the CALIPSO classification scheme. Finally, the seasonal distribution of the vertical distribution of the extinction for each LIVAS cell was provided. A schematic outline of the LIVAS processing chain is given in Figure 9.

## 4. Results and discussion

### 4.1. LIVAS products

The final LIVAS aerosol/cloud database contains multi-wavelength 4-year averaged vertical distributions and statistics for a global grid of 1x1 degree. Here, we demonstrate the LIVAS products through an example for one grid cell corresponding to our hometown, Athens, in Greece (centroid latitude of 38.5$^{o}$ North and longitude of 23.5$^{o}$ East).

In the upper panel of Figure 10 the aerosol extinction is given for the LIVAS lidar wavelengths, i.e. 355, 532, 1064, 1570, 2050 nm, along with the standard deviation of the averaging at 532 nm (grey line). The number of observations is presented in the right panel for each plot, in order to have a measure of the representativeness of the mean aerosol extinction for each cell, which depends on the available CALIPSO overpasses and corresponding samples. The maximum surface elevation over the

CALIPSO overpass is given for the grid cell of interest, as obtained from the digital elevation map (DEM) used by CALIPSO. In the middle panel of Figure 10, the mean extinction profile is given per CALIPSO aerosol type, while in the lower panel the mean extinction is given per season with the corresponding sampling/occurrences used for their production.

Additional LIVAS products are provided for particle depolarization at 532 nm. These refer to the mean particle depolarization along with its standard deviation (Figure 11 – upper panel). Moreover, mean cloud extinction at 532 nm is given in LIVAS (Figure 11 – middle panel) along with mean extinction coefficient of stratospheric features in total (Figure 11 – lower panel) but also for PSCs and aerosol particles separately.

Finally, for each grid cell a number of statistical parameters are provided in LIVAS regarding the mean, minimum and maximum surface elevation, the number of overpasses for each cell, the number of examined profiles, the samples averaged after filtering (total, aerosol, clear air), the subtype occurrence in the aerosol total observations (in percentages) and the AOD at 532 nm (mean, median and standard deviation).

**4.2 LIVAS AOD evaluation**

In this section an evaluation of the LIVAS climatological AOD mean values at 532 nm is given, using collocated AERONET AOD averages. AERONET stations included in each grid cell of 1x1 degree were considered representative when the stations were operated for the same time period with LIVAS (2008-2011). LIVAS mean AOD was calculated by the integration of the 4-year-averaged extinction profile, while AERONET AOD was calculated by averaging all available station data. A first comparison of LIVAS AODs against AERONET is presented in Figure 12. Blue circles denote the absolute value of the difference (LIVAS mean – AERONET mean), while the red crosses denote the elevation difference between the AERONET site and the

mean elevation of the CALIPSO ground track. This map provides only the magnitude of biases (absolute values) to demonstrate the range of discrepancies with respect to the elevation slope. Large differences can also be attributed to specific grid cell under-sampling by CALIPSO in the 4-year period, as discussed below.

Large elevation differences may cause large AOD biases since in such cases the optical path lengths monitored by AERONET and CALIPSO instruments can vary. Moreover, when CALIPSO overpasses high-slope terrains, the sampling may become inadequate for heights lower than the maximum elevation. An example of such a case is given in Figure 13 for the AERONET station of "ND_Marbel_Univ" in Philippines. CALIPSO overpasses this station over elevations ranging from zero to 1.46 km. The number of observations for heights lower than the maximum elevation becomes very small (Figure 13 – right panel) and inadequate for statistical purposes. This under-sampling affected the final averaged extinction profile as shown in the left panel of Figure 13 for heights lower than the maximum elevation. In order to eliminate these effects from the comparison of LIVAS with AERONET, we applied on our dataset the following constraints:

1) The elevation difference between the AERONET site and CALIPSO mean ground track elevation was kept below 100 m.

2) The elevation slope in CALIPSO overpass was constrained to be less than 400 m.

3) CALIPSO sampling was controlled by constraining the comparison over grid cells with large number of overpasses, i.e. over 150.

The third constraint is considered crucial for the representativeness of LIVAS database. As shown in Figure 14, in approximately 30% of the global 1x1 degree cells of the database the number of overpasses is less than 150. This under-sampling along with possible high-slope terrains could cause unrealistic results.

Figure 15 presents the absolute bias of the means for our constrained dataset (i.e. averaged CALIPSO AOD minus the averaged AERONET AOD). For most sites the comparison reveals biases within ±0.1 in terms of AOD. Negative LIVAS biases lower than -0.1 (denoted in Figure 15 with blue color) were found mostly over the Saharan desert, a result that may be related to possible CALIPSO underestimations for dust as already reported in the literature (e.g. Wandinger et al., 2010; Schuster et al., 2012; Tesche et al., 2013; Amiridis et al., 2013). Positive LIVAS biases larger than 0.1 denoted with red color in Figure 15 were mostly found over coastlines. This effect is not well understood yet. Campbell et al. (2012) found CALIPSO offsets over coastlines when comparing with the U.S. Naval Aerosol Analysis and Predictive System (NAAPS). Recently, Kanitz et al. (2014) found a systematic overestimation of the AOD over land in coastal areas of up to a factor of 3.5. The researchers attribute the possible CALIPSO overestimation to the surface-dependent criterion (land/ocean) included in the classification scheme which may prohibit a correct classification of sea-breeze-related marine aerosol over land, leading to unrealistically high lidar ratio assumptions.

We have to mention here that the LIVAS validation presented in Figure 15 cannot be conclusive on the aforementioned possible issues. Overall, the global LIVAS agreement with AERONET within 0.1 AOD is considered a very good result for a 4-year product. Keeping the constrained dataset for a quantitative comparison, we present in Figure 16 scatter plots for AOD averages at the different LIVAS wavelengths. In the upper panel we show the comparison for the averaged AOD at 532 nm (left) and for the standard deviation of the distribution (right). A Pearson correlation coefficient of 0.86 reveals a very good agreement for the AOD at 532 nm. The slope of the linear regression is 0.79, showing a slight underestimation of the LIVAS AOD. Since the

532 nm LIVAS products come directly from CALIPSO averages, this underestimation is probably related to CALIPSO limitations (e.g. Schuster et al., 2012; Omar et al., 2013). The variability of the CALIPSO samples averaged for LIVAS is consistent with AERONET as shown in the upper right panel of Figure 16. The LIVAS AOD at 355 nm (lower left panel) is also in a very good agreement with AERONET, showing similar values of Pearson's r and slope as those of the 532 nm comparison. This result shows that the conversion of the CALIPSO extinction product from 532 to 355 nm was successful using the EARLINET conversion factors. Regarding the comparison at IR wavelengths (lower right panel), the results were not encouraging. LIVAS AOD at 1570 nm is consistent with AERONET for AODs lower than 0.1 but not for higher values where LIVAS heavily underestimates. This can be attributed to errors introduced due to the extrapolation of the AERONET AOD in the IR (note that we used AERONET AOD measurements at 440, 670, 860 and 1020 nm), and/or to uncertainties introduced by the LIVAS conversion scheme in the IR.

**4.3 LIVAS web-portal**

The LIVAS database is freely available under the url: http://lidar.space.noa.gr:8080/livas/, where the database is stored and exposed (Figure 17). The webpage provides the complete information on the methodological approaches and instructions on portal's usage. The data are provided in ASCII and netcdf formats, while brief statistics and quick-view charts are projected online. The user can select to download the database via ftp, or navigate to the region of interest by using a dynamic map to select over the World grid of 1x1 degree spatial resolution. The map provides the possibility to overlay a layer that represents the number of CALIPSO overpasses. This is considered crucial for the use of the database since only grid cells with a number of CALIPSO overpasses greater than 150 are recommended

for their statistical representativeness. Moreover, the user can overlay global AODs or cloud optical depths on the map. In the example of Figure 18, the global distribution of LIVAS AODs is presented, showing high values over well-known sources like the dust belt, India and China as well as transport paths as the one from Sahara westward across the Atlantic.

## 5. Summary and conclusions

We presented LIVAS, a 4-year multi-wavelength global aerosol and cloud optical database that has been developed for complementing existing datasets used by ESA for instrument performance simulation of current and future space-borne lidars as well as retrieval algorithm testing activities based on realistic atmospheric scenarios. In order to cover the different spectral domains for HSRL and IPDA lidars, the compiled database addresses the three harmonic operating wavelengths of Nd-YAG lasers (355, 532 and 1064 nm) as well as typical wavelengths of IPDA lidars in the SWIR spectral domain (1570 and 2050 nm).

When compared to AERONET, the LIVAS AOD values appeared to be realistic and representative for VIS wavelengths but also for UV, making this database appropriate for use by ADM-Aeolus and EarthCARE. Regarding the IR conversion however, LIVAS is not considered representative when compared to AERONET, especially for AODs higher than 0.1. We believe that LIVAS is representative in the UV due to the fact that BAE and EAE were provided by ground-based lidar measurements of high quality as those provided by EARLINET. Moreover, the methodology used for the application of the conversions was based on aerosol classification advances developed within the ESA-CALIPSO project. For IR however, BAE and EAE were not measured but they were calculated from scattering simulations using typical size distributions and refractive indexes assumed for each CALIPSO aerosol type, deduced from

AERONET data and aerosol models provided in the literature. Even though EARLINET was used to constrain the IR simulations, the final results were not satisfactory and more work is needed that would benefit from potential future IR ground-based measurements. However, the LIVAS aerosol model found to be more consistent with ESA-CALIPSO but also the relative literature than the one used by CALIPSO for the UV-VIS spectral region, especially for the BAE.

In the future, we plan to expand LIVAS in monthly-averaged aggregations in order to provide timeseries for UV lidar products. In this way, LIVAS timeseries could be homogenized in the future with EarthCARE products for the consolidation of a multi-year aerosol/cloud multi-wavelength 4D dataset appropriate for climate studies. However, the challenges for this task are significant, due to a number of open scientific questions and related knowledge gaps. Specifically, the homogenization scheme envisaged cannot be realized without defining a common aerosol/cloud model that will be applicable to all the missions. This includes also the definition of a common aerosol/cloud classification scheme for the space-borne products and ancillary ground-based datasets and the derivation of aerosol/cloud-type-dependent AE for all lidar-related properties, i.e., extinction, backscatter and depolarization. It is believed that the well-established EARLINET network offers a unique opportunity to support such an effort. Several EARLINET stations operate multi- wavelength Raman lidars, with most of them measuring particle depolarization as well. Network's so-called "core stations" deliver the entire CALIOP/ALADIN/ATLID parameter set, so that conversion factors for a variety of aerosol types can be derived experimentally over a comparably long time period.

## ACKNOWLEDGMENTS

This work has been developed under the auspices of the ESA-ESTEC project: Lidar Climatology of Vertical Aerosol Structure for Space-Based LIDAR Simulation Studies (LIVAS) contract N°4000104106/11/NL/FF/fk. The publication was supported by the European Union Seventh Framework Programme (FP7-REGPOT-2012-2013-1), in the framework of the project BEYOND, under Grant Agreement No. 316210 (BEYOND - Building Capacity for a Centre of Excellence for EO-based monitoring of Natural Disasters). The research leading to these results has received funding from the European Union Seventh Framework Programme (FP7/2007-2013) under grant agreement no 262254 (ACTRIS), grant agreement n° 606953 and grant agreement no 289923 – ITaRS. This research has been financed by EPAN II and PEP under the national action "Bilateral, multilateral and regional R&T cooperations" (AEROVIS Sino-Greek project). This work was performed in the framework of PROTEAS project within GSRT's KRIPIS action, funded by Greece and the European Regional Development Fund of the European Union under the O.P. Competitiveness and Entrepreneurship, NSRF 2007-2013 and the Regional Operational Program of Attica.

The authors acknowledge EARLINET for providing aerosol lidar profiles available under the World Data Center for Climate (WDCC) ("The EARLINET publishing group 2000-2010, 2014 a, b, c, d, e). We thank the AERONET PIs and their staff for establishing and maintaining the AERONET sites used in this investigation. CALIPSO data were obtained from the ICARE Data Center (http://www.icare.univ-lille1.fr/). We would like to thank Jason Tackett for his support during the algorithm development for the production of Level 3 CALIPSO products.

# TABLES

**Table 1.** LIVAS aerosol model microphysical parameters.

| aerosol type | LIVAS model microphysical parameters | | | | | | | | | |
|---|---|---|---|---|---|---|---|---|---|---|
| | Size distribution parameters | | | | | | Refractive index at 532 nm | | | |
| | fine mode | | | coarse mode | | | fine mode | | coarse mode | |
| | median radius (μm) | standard deviation | total volume ($\mu m^3/\mu m^2$) | median radius (μm) | standard deviation | total volume (μm3/μm2) | real part | imag. part | real part | imag. part |
| **polluted continental** | 0.2 | 0.5 | 0.08 | 2.8 | 0.68 | 0.05 | 1.45 | 0.006 | 1.45 | 0.006 |
| **smoke** | 0.17 | 0.5 | 0.05 | 3.7 | 0.65 | 0.03 | 1.47 | 0.018 | 1.47 | 0.018 |
| **dust** | 0.14 | 0.5 | 0.04 | 2.2 | 0.68 | 0.25 | 1.51 | 0.022 | 1.51 | 0.022 |
| **polluted dust** | 0.17 | 0.57 | 0.14 | 3.2 | 0.67 | 0.19 | 1.49 | 0.017 | 1.49 | 0.017 |
| **clean marine** | 0.16 | 0.5 | 0.22 | 2.6 | 0.72 | 1.5 | 1.41 | 0.002 | 1.36 | 0 |
| **clean continental** | 0.2 | 0.8 | 0.94 | 5.97 | 0.92 | 0.6 | 1.42 | 0.0023 | 1.53 | 0.008 |

**Table 2.** LIVAS and CALIPSO aerosol models.

| aerosol type | LIVAS aerosol model | | | CALIPSO aerosol model | | |
|---|---|---|---|---|---|---|
| | **LR at 532 nm (sr)** | **SSA at 532 nm** | **effective radius (μm)** | **LR at 532 nm (sr)** | **SSA at 532 nm** | **effective radius (μm)** |
| **polluted continental** | 64 | 0.95 | 0.28 | 70 | 0.93 | 0.26 |
| **smoke** | 90 | 0.88 | 0.26 | 70 | 0.8 | 0.36 |
| **dust** | 85 | 0.87 | 0.65 | 40 | 0.9 | 0.43 |
| **polluted dust** | 82 | 0.89 | 0.35 | 65 | 0.8 | 0.43 |
| **clean marine** | 31 | 0.98 | 0.75 | 20 | 0.99 | 0.93 |
| **clean continental** | 54 | 0.96 | 0.26 | 35 | 0.88 | 1.4 |

**Table 3.** BAE and EAE for each aerosol type used in LIVAS for the conversion from 532 to 355 nm (VIS-UV) and from 532 to 1570 and 2050 nm (VIS-IR). The approaches used for their calculation are also indicated.

| LIVAS AEROSOL TYPE | UV/VIS | | | VIS/IR | | | | |
|---|---|---|---|---|---|---|---|---|
| | approach used | 532/355 nm | | approach used | 532/1570 nm | | 532/2050 nm | |
| | | BAE | EAE | | BAE | EAE | BAE | EAE |
| **Polluted continental** | ESA-CALIPSO | 1.42 | 1.24 | AERONET-Omar | 1.18 | 1.66 | 1.32 | 1.56 |

| | | | | | | | | |
|---|---|---|---|---|---|---|---|---|
| **Dust** | ESA-CALIPSO | 0.40 | 0.55 | AERONET-CALIPSO | 0.35 | 0.6 | 0.43 | 0.57 |
| **Polluted dust** | ESA-CALIPSO | 0.92 | 0.71 | AERONET-CALIPSO | 0.67 | 1.14 | 0.71 | 1.07 |
| **Smoke** | ESA-CALIPSO | 1.46 | 1.41 | AERONET-CALIPSO | 0.79 | 1.42 | 0.825 | 1.34 |
| **Clean marine** | ESA-CALIPSO (bsc) Sayer et al. (2012) (ext) | 0.50 | 0.78 | Sayer et al. (2012) | 0.74 | 0.39 | 0.81 | 0.38 |
| **Clean continental** | ESA-CALIPSO (bsc) OPAC (ext) | 1.20 | 1.31 | OPAC | 1.15 | 1.28 | 1.64 | 1.27 |
| **Stratospheric** | ESA-CALIPSO (bsc) Deshler et al. (1993), Wandinger et al. (1995) (ext) | 0.98 | 0.48 | Deshler et al. (1993), Wandinger et al. (1995) | 1.36 | 1.33 | 1.38 | 1.49 |

1

2

## FIGURE CAPTIONS

**Figure 1.** The data and methods used for the derivation of LIVAS BAE and EAE in the UV and IR.

**Figure 2:** BAE (upper) and EAE (bottom) calculated with different approaches (i.e. "AERONET-Omar" (red triangles), "AERONET-CALIPSO" (green triangles), "Sayer et al., (2012)" (cyan triangles), "OPAC" (pink triangles)) and validated against the ESA-CALIPSO BAE and EAE in VIS and UV (black circles). The BAE and EAE selected and ingested in the LIVAS aerosol model for the VIS-IR conversions, are denoted with symbols of larger size.

**Figure 3:** Comparison of the mean volume size distributions for each aerosol type in the LIVAS (blue line) and CALIPSO (pink line) aerosol models.

**Figure 4:** Comparison of the mean real part of the refractive index for each aerosol type in the LIVAS (blue line) and CALIPSO (pink line) aerosol models.

**Figure 5:** Comparison of the mean imaginary part of the refractive index for each aerosol type in the LIVAS (blue line) and CALIPSO (pink line) aerosol models.

**Figure 6:** Comparison of the mean spectral SSA for each aerosol type in the LIVAS (blue line) and CALIPSO (pink line) aerosol models.

**Figure 7:** Comparison of the LIVAS and CALIPSO aerosol models with ESA-CALIPSO values for: BAE at 355/532 nm (upper-left), EAE at 355/532 nm (upper-right), lidar ratio at 532 nm (lower-left) and effective radius (lower-right).

**Figure 8:** CALIPSO Level 2 extinction coefficient profile at 532 nm (left), aerosol type (center) and converted extinction coefficient at 355 nm (right), based on LIVAS typical EAE. The profile example refers to September 7$^{th}$, 2011, (cell centroid with latitude of 37.5 and longitude of 20.5 degrees).

**Figure 9.** Schematic diagram of LIVAS processing chain.

**Figure 10.** LIVAS aerosol extinction products. Upper panel: vertical distribution of the averaged aerosol extinction coefficient at 355, 532, 1064, 1570, 2050 nm (left), number of observations used in averaging (right). Middle panel: vertical distribution of the averaged aerosol extinction coefficient per aerosol type (left), number of observations used in averaging (right). Lower panel: vertical distribution of the averaged aerosol extinction coefficient per season (left), number of observations used in averaging (right).

**Figure 11.** Additional LIVAS products: Upper panel: vertical distribution of the averaged particle depolarization at 532 nm (left), number of observations used in averaging (right). Middle panel: vertical distribution of the averaged cloud extinction coefficient per season (left), number of observations used in averaging (right). Lower panel: vertical distribution of the averaged stratospheric aerosol extinction coefficient (left), number of observations used in averaging (right).

**Figure 12.** Spatial distribution of the 532 nm AOD absolute differences (absolute value of LIVAS averaged AOD minus AERONET averaged AOD) (blue circles) and of the difference between AERONET site elevation and mean grid cell elevation of CALIPSO overpass (red crosses).

**Figure 13.** Example of high-slope terrain on CALIPSO overpass for the case of ND_Marbel_Univ AERONET station. Left panel: vertical distribution of the averaged aerosol extinction coefficient. Right panel: number of observations used in averaging.

**Figure 14.** Percentiles of the number of overpasses in LIVAS global grid cells.

**Figure 15.** Spatial distribution of the 532 nm AOD absolute biases (LIVAS averaged AOD minus AERONET averaged AOD).

**Figure 16.** Upper panel: Scatter plot comparison of LIVAS AODs at 532 nm versus collocated AERONET Level 2 product (left) and standard deviation of the LIVAS AODs versus standard deviation of the AERONET AODs at 532 nm (right). Lower panel: Scatter plot comparison of LIVAS AODs at 355 nm versus collocated AERONET Level 2 product (left) and of LIVAS AODs at 1570 nm versus collocated AERONET Level 2 product (right).

**Figure 17.** The LIVAS web-portal.

**Figure 18.** Global distribution of LIVAS AOD at 532 nm.

## FIGURES

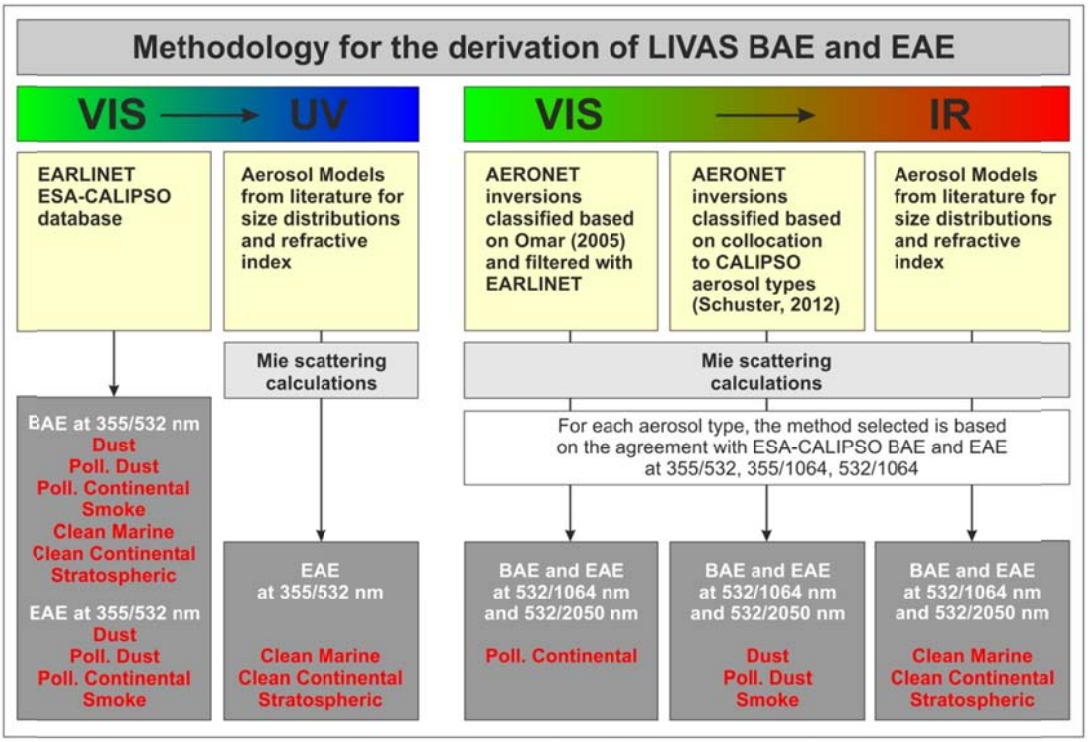


**Figure 1**

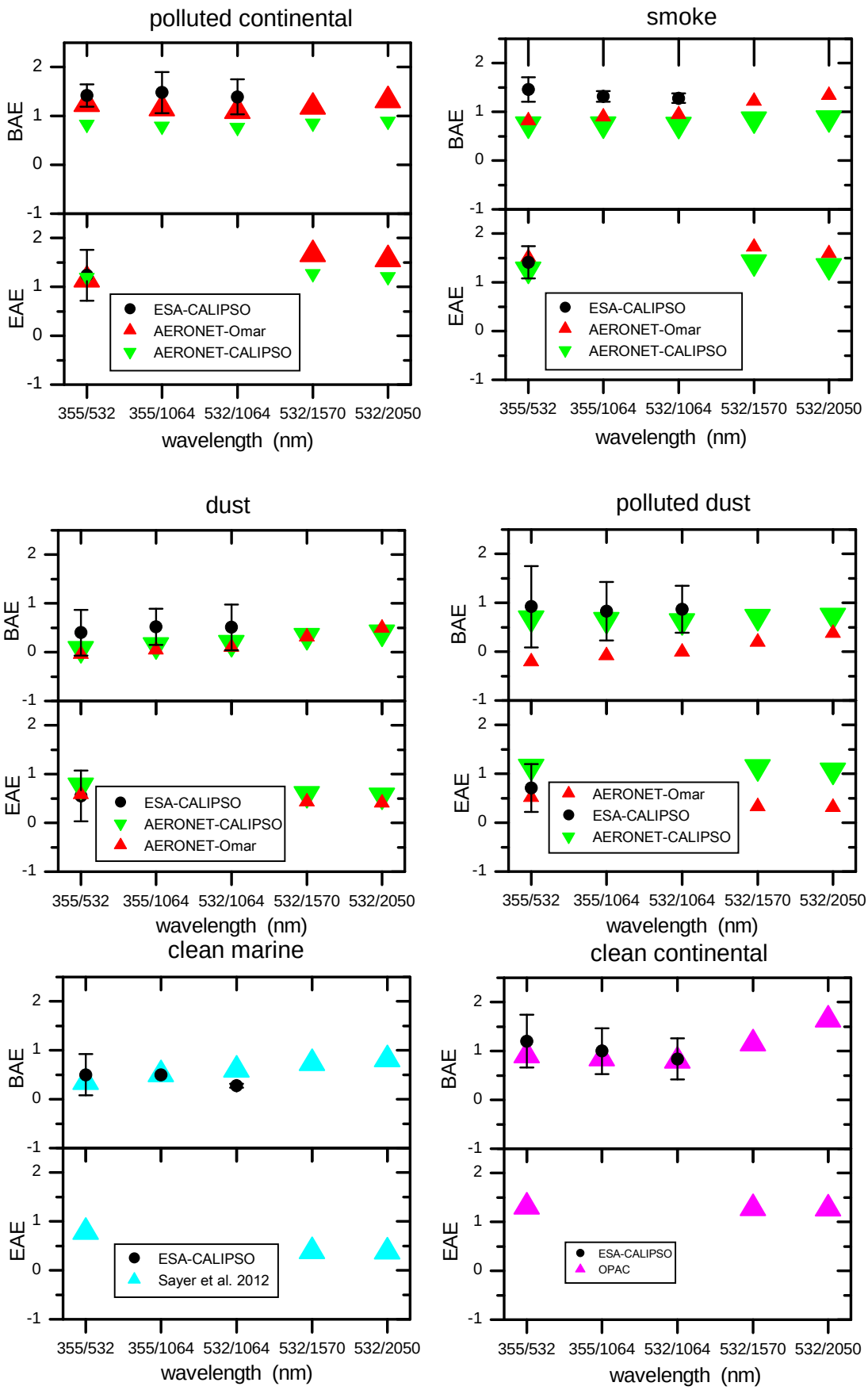
polluted continental
smoke
dust
polluted dust
clean marine
clean continental
BAE
EAE
wavelength (nm)
355/532
355/1064
532/1064
532/1570
532/2050
ESA-CALIPSO
AERONET-Omar
AERONET-CALIPSO
Sayer et al. 2012
OPAC

**Figure 2**

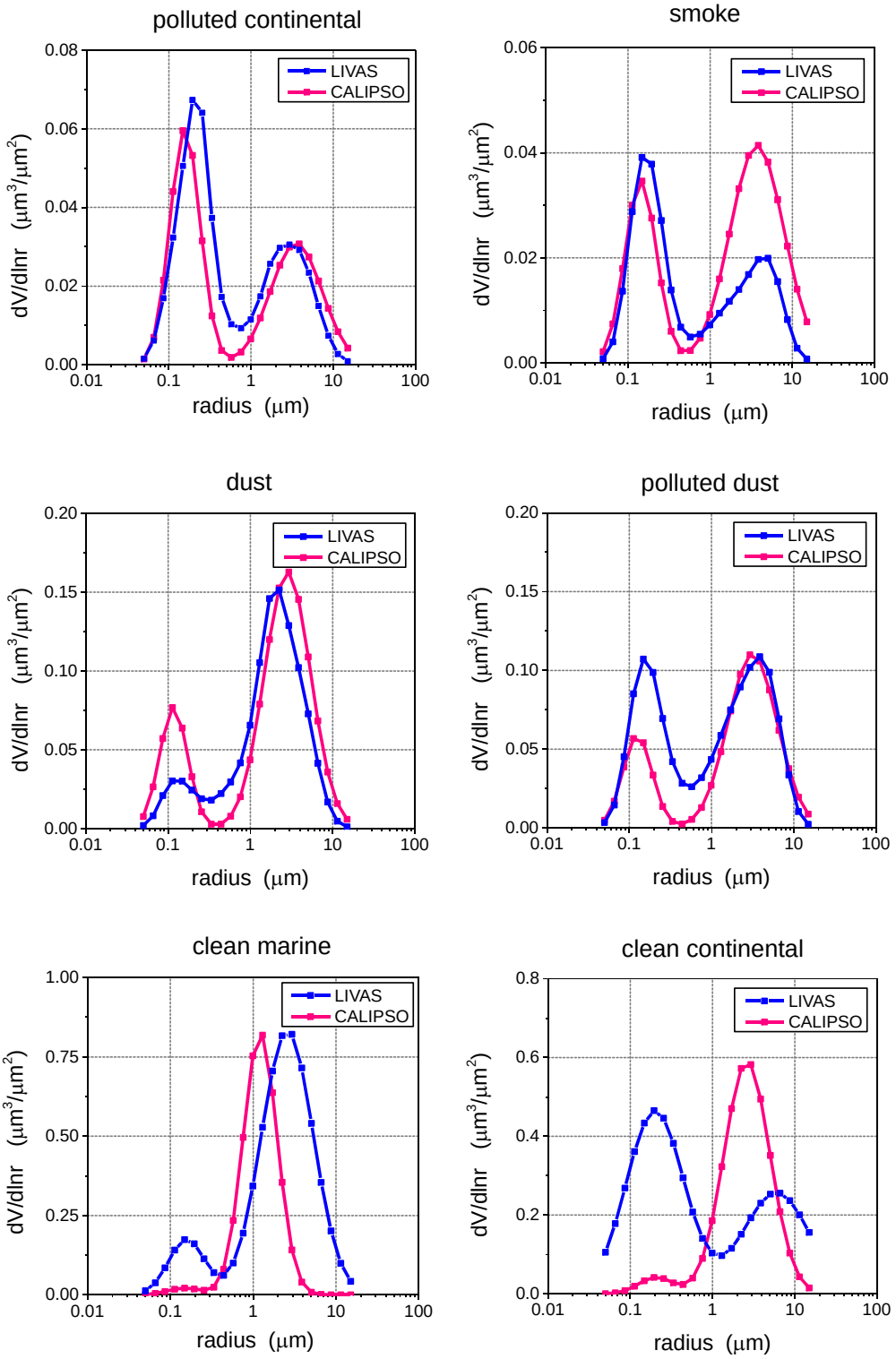
polluted continental
smoke
dust
polluted dust
clean marine
clean continental
LIVAS
CALIPSO
dV/dlnr (μm³/μm²)
radius (μm)

**Figure 3**

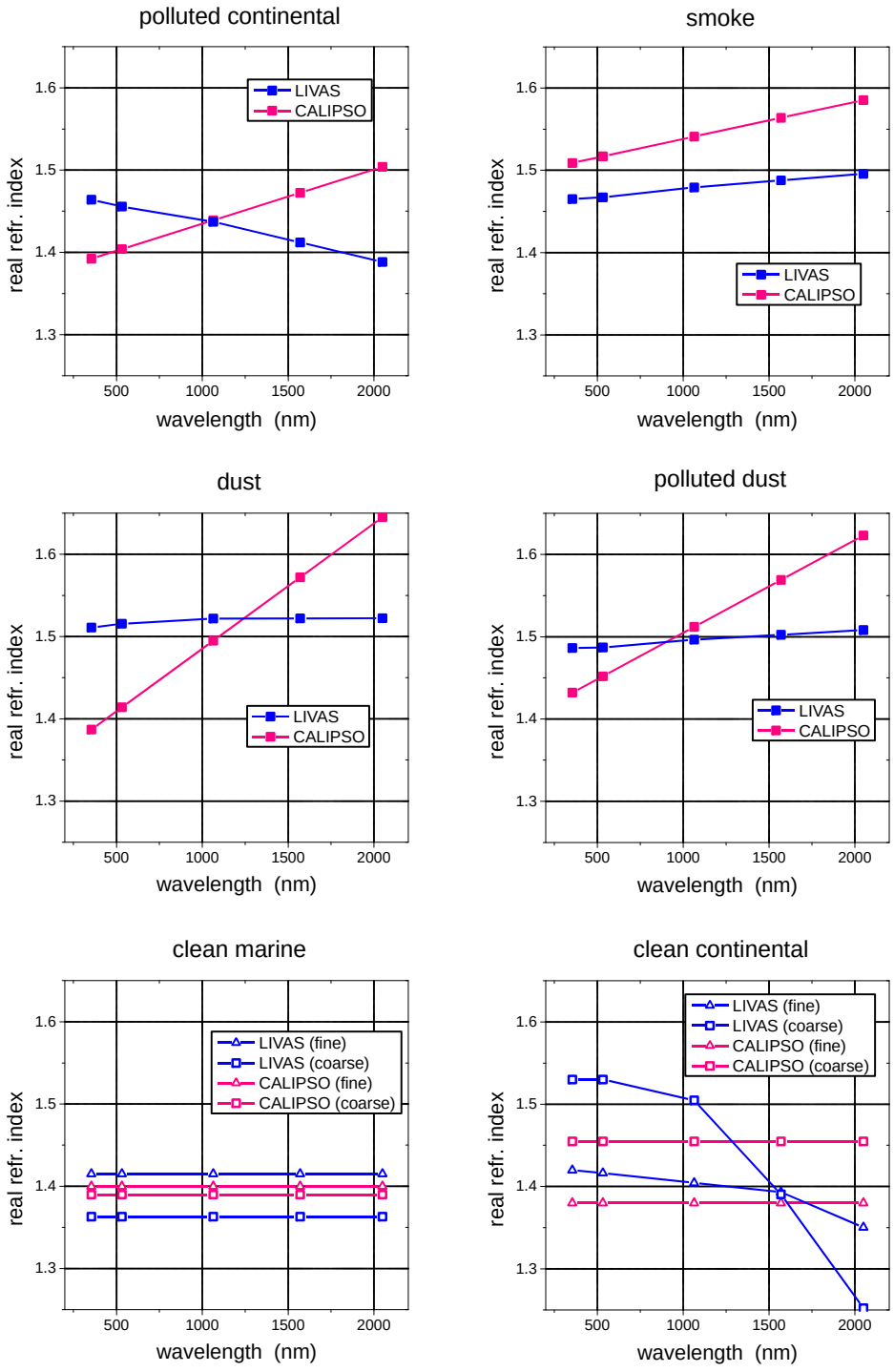
polluted continental
LIVAS
CALIPSO
real refr. index
wavelength (nm)
smoke
dust
polluted dust
clean marine
LIVAS (fine)
LIVAS (coarse)
CALIPSO (fine)
CALIPSO (coarse)
clean continental

**Figure 4**

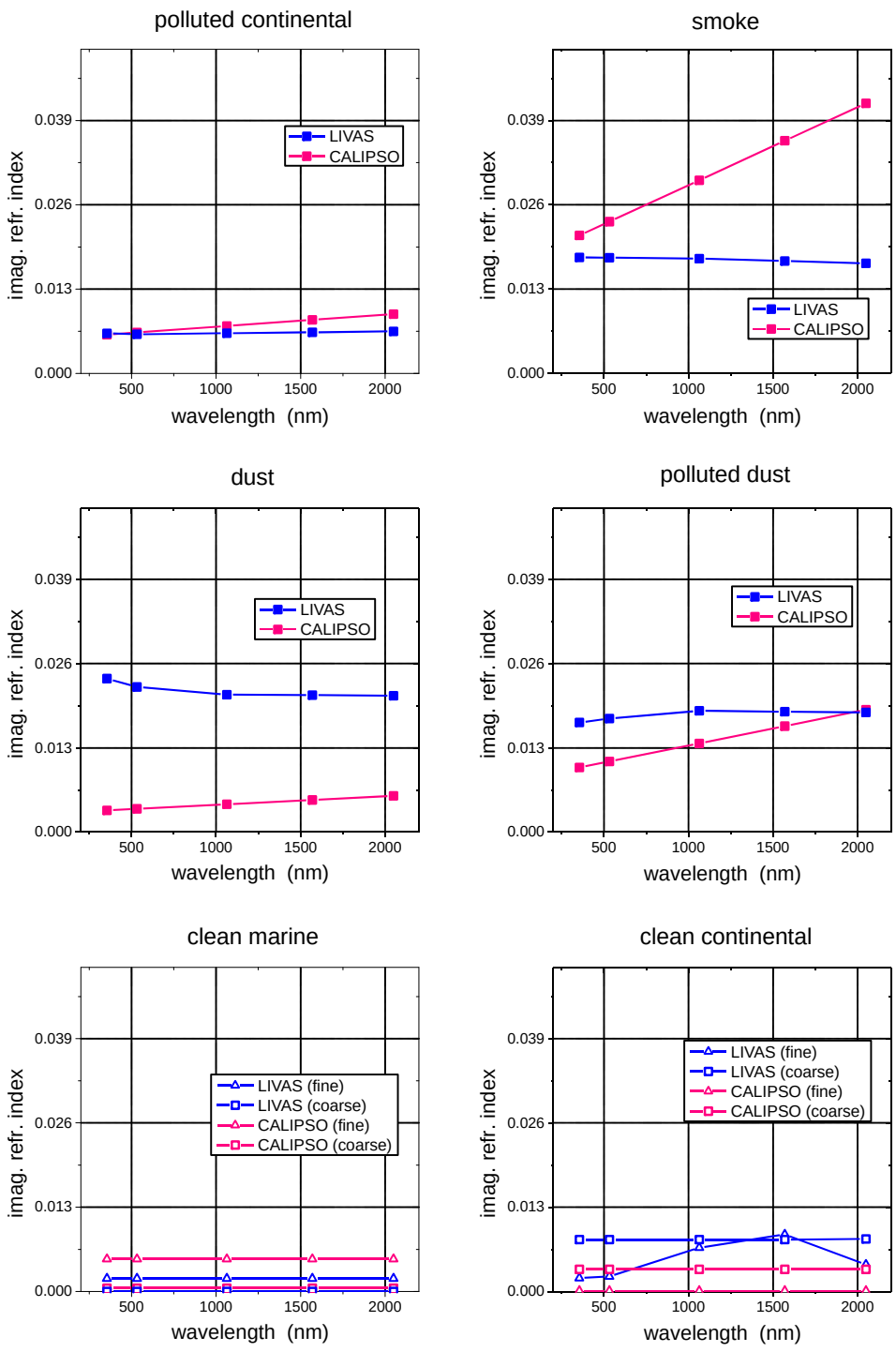
polluted continental
smoke
dust
polluted dust
clean marine
clean continental
imag. refr. index
wavelength (nm)
0.000
0.013
0.026
0.039
500
1000
1500
2000
LIVAS
CALIPSO
LIVAS (fine)
LIVAS (coarse)
CALIPSO (fine)
CALIPSO (coarse)

**Figure 5**

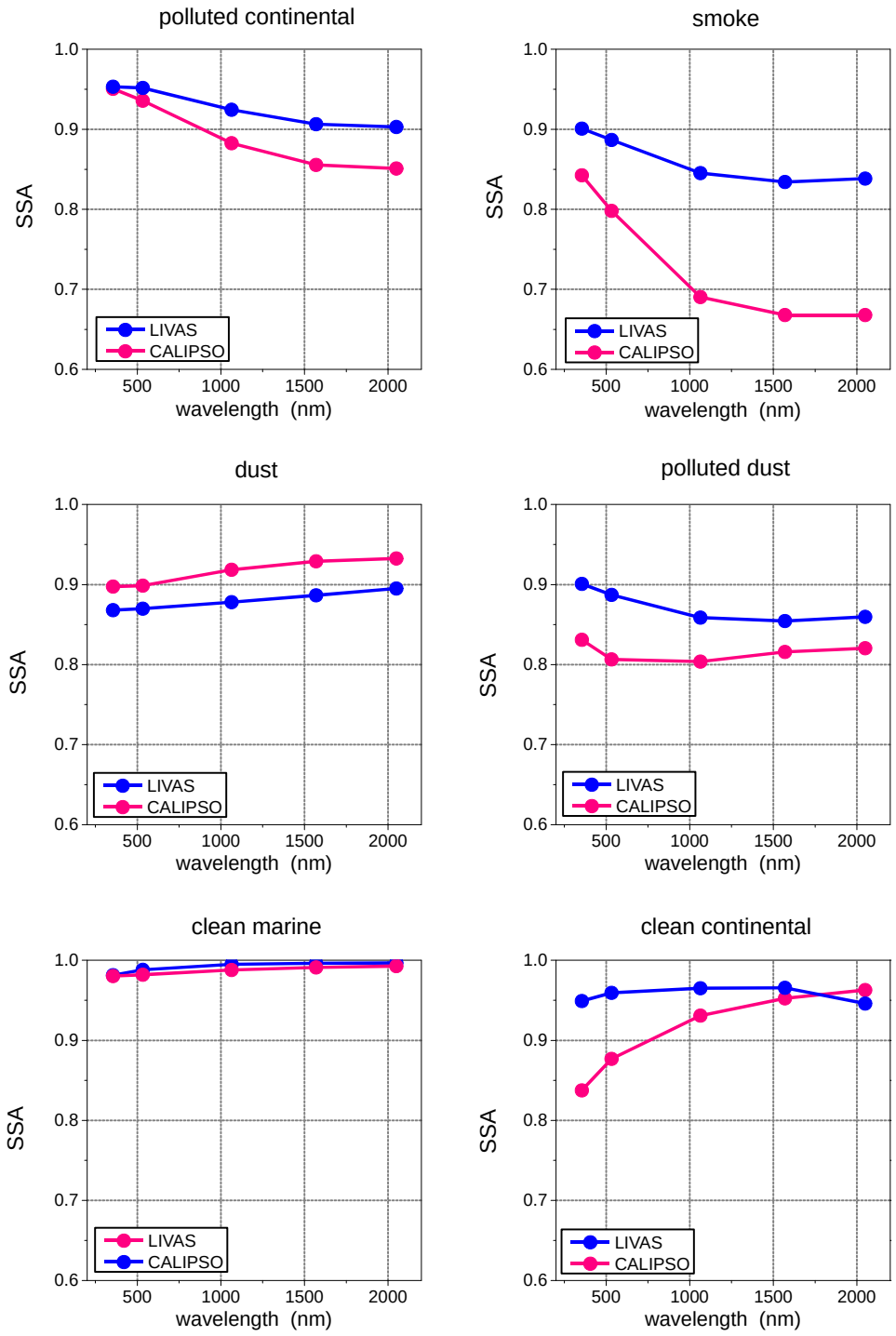
polluted continental
smoke
dust
polluted dust
clean marine
clean continental
SSA
wavelength (nm)
LIVAS
CALIPSO
1.0
0.9
0.8
0.7
0.6
500
1000
1500
2000

**Figure 6**

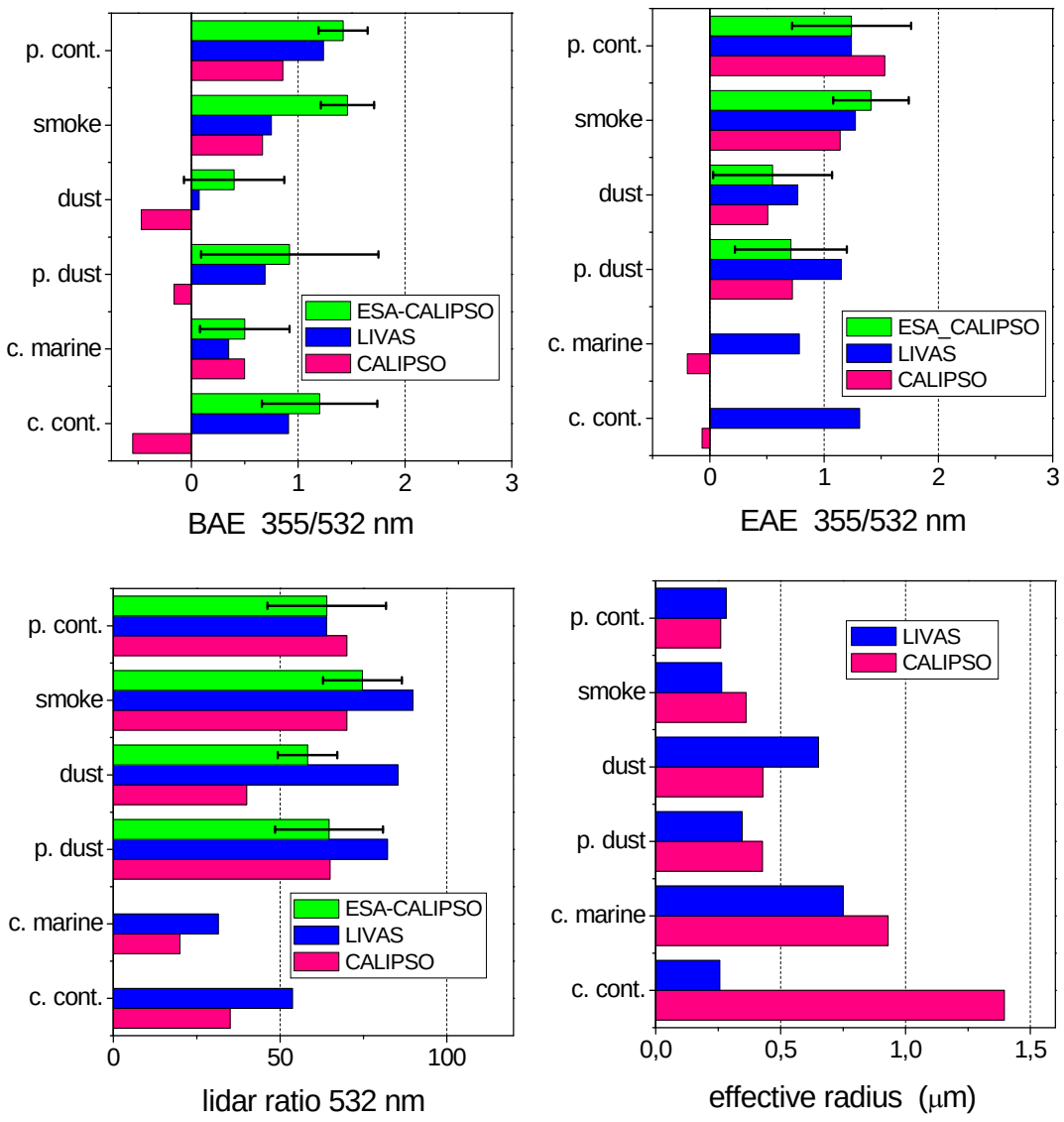
p. cont.
smoke
dust
p. dust
c. marine
c. cont.
ESA-CALIPSO
LIVAS
CALIPSO
0
1
2
3
BAE 355/532 nm
ESA_CALIPSO
LIVAS
CALIPSO
EAE 355/532 nm
0
50
100
lidar ratio 532 nm
0,0
0,5
1,0
1,5
effective radius (μm)

**Figure 7**

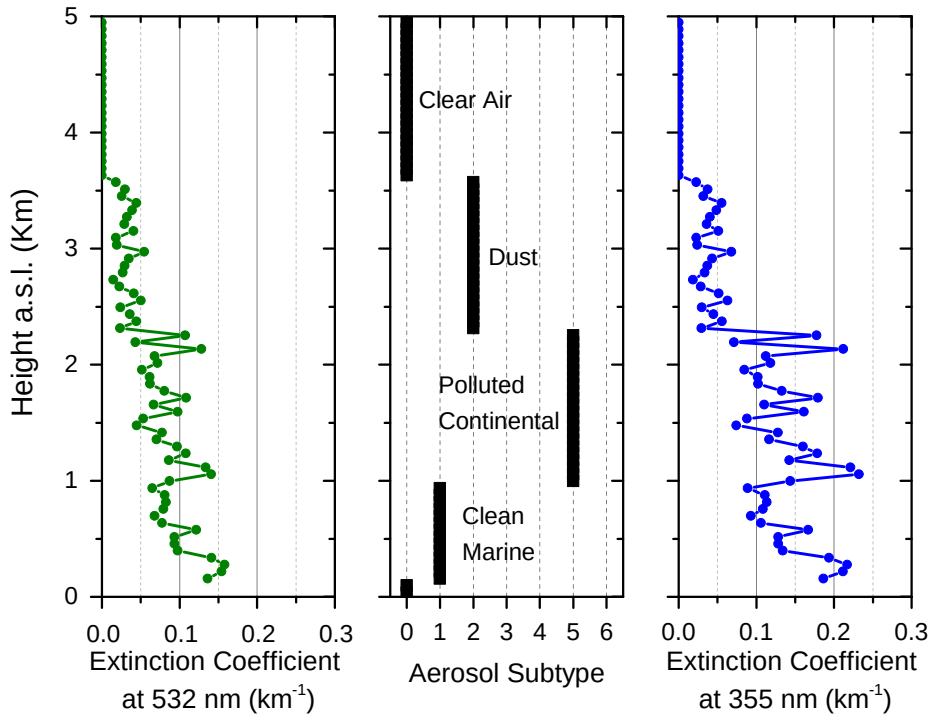
Height a.s.l. (Km)
0
1
2
3
4
5
0.0
0.1
0.2
0.3
Extinction Coefficient
at 532 nm (km-1)
Clear Air
Dust
Polluted
Continental
Clean
Marine
0
1
2
3
4
5
6
Aerosol Subtype
0.0
0.1
0.2
0.3
Extinction Coefficient
at 355 nm (km-1)

**Figure 8**

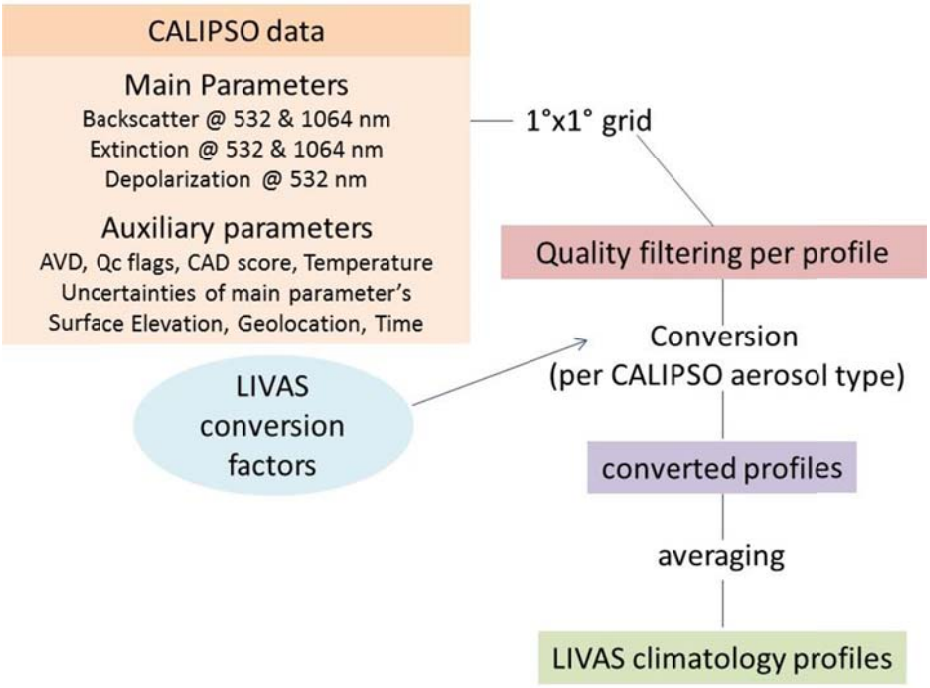
CALIPSO data
Main Parameters
Backscatter @ 532 & 1064 nm
Extinction @ 532 & 1064 nm
Depolarization @ 532 nm
Auxiliary parameters
AVD, Qc flags, CAD score, Temperature
Uncertainties of main parameter's
Surface Elevation, Geolocation, Time
1°x1° grid
Quality filtering per profile
Conversion
(per CALIPSO aerosol type)
LIVAS
conversion
factors
converted profiles
averaging
LIVAS climatology profiles

**Figure 9**

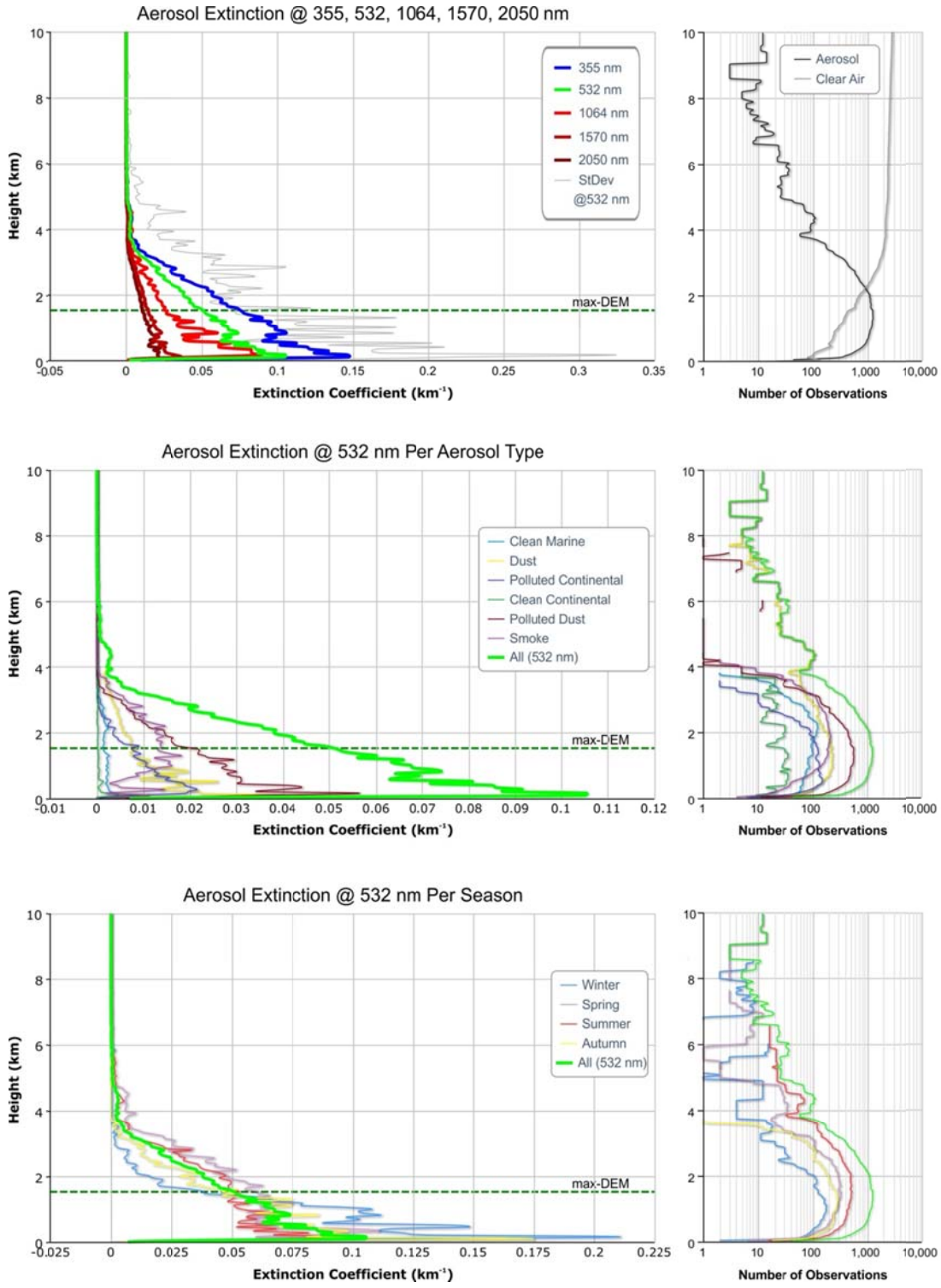
Aerosol Extinction @ 355, 532, 1064, 1570, 2050 nm
355 nm
532 nm
1064 nm
1570 nm
2050 nm
StDev @532 nm
max-DEM
Height (km)
Extinction Coefficient (km⁻¹)
Aerosol
Clear Air
Number of Observations
Aerosol Extinction @ 532 nm Per Aerosol Type
Clean Marine
Dust
Polluted Continental
Clean Continental
Polluted Dust
Smoke
All (532 nm)
max-DEM
Height (km)
Extinction Coefficient (km⁻¹)
Number of Observations
Aerosol Extinction @ 532 nm Per Season
Winter
Spring
Summer
Autumn
All (532 nm)
max-DEM
Height (km)
Extinction Coefficient (km⁻¹)
Number of Observations

**Figure 10**

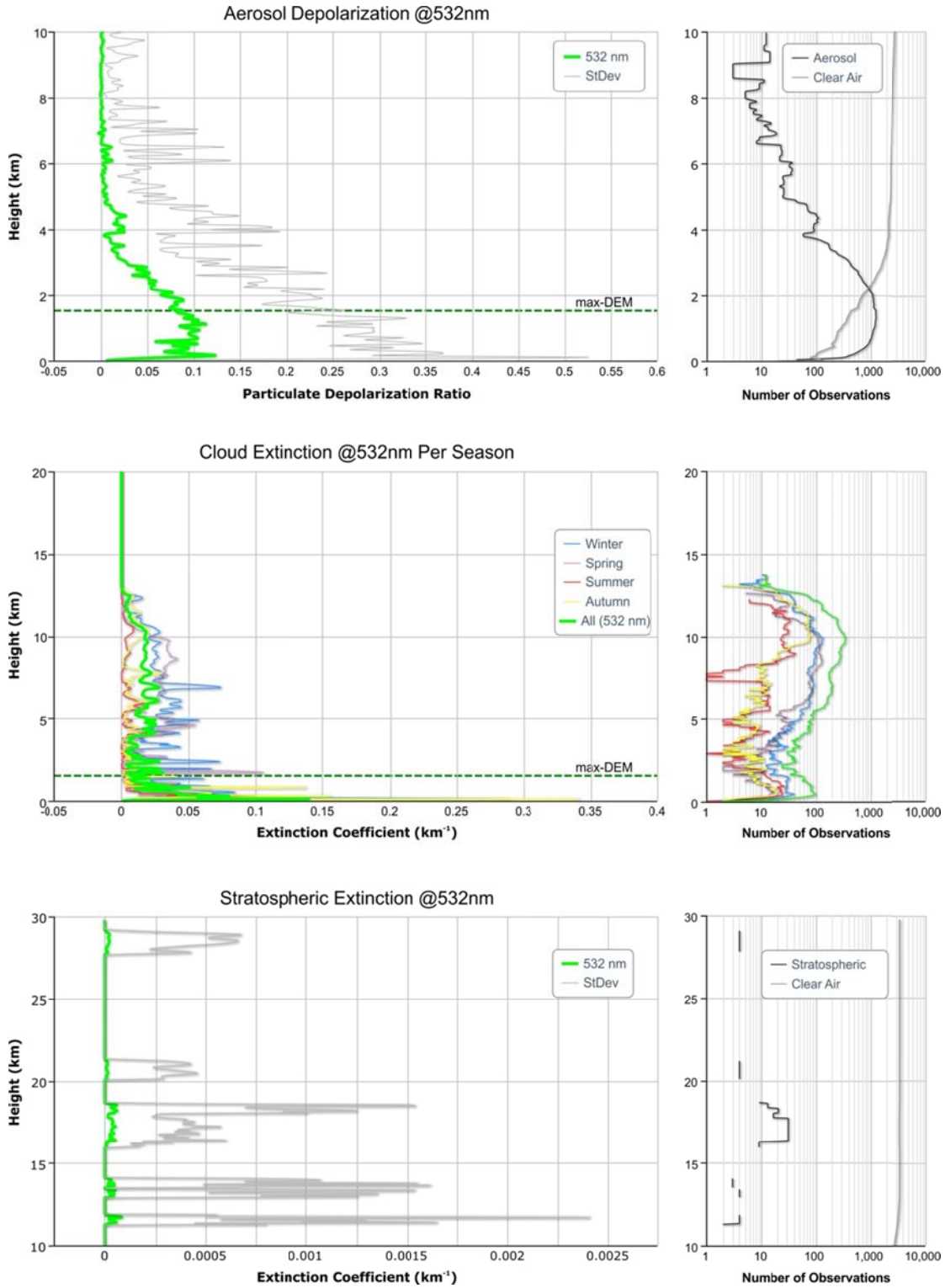
Aerosol Depolarization @532nm
532 nm
StDev
max-DEM
Height (km)
Particulate Depolarization Ratio
Aerosol
Clear Air
Number of Observations
Cloud Extinction @532nm Per Season
Winter
Spring
Summer
Autumn
All (532 nm)
max-DEM
Height (km)
Extinction Coefficient (km⁻¹)
Number of Observations
Stratospheric Extinction @532nm
532 nm
StDev
Height (km)
Extinction Coefficient (km⁻¹)
Stratospheric
Clear Air
Number of Observations

**Figure 11**

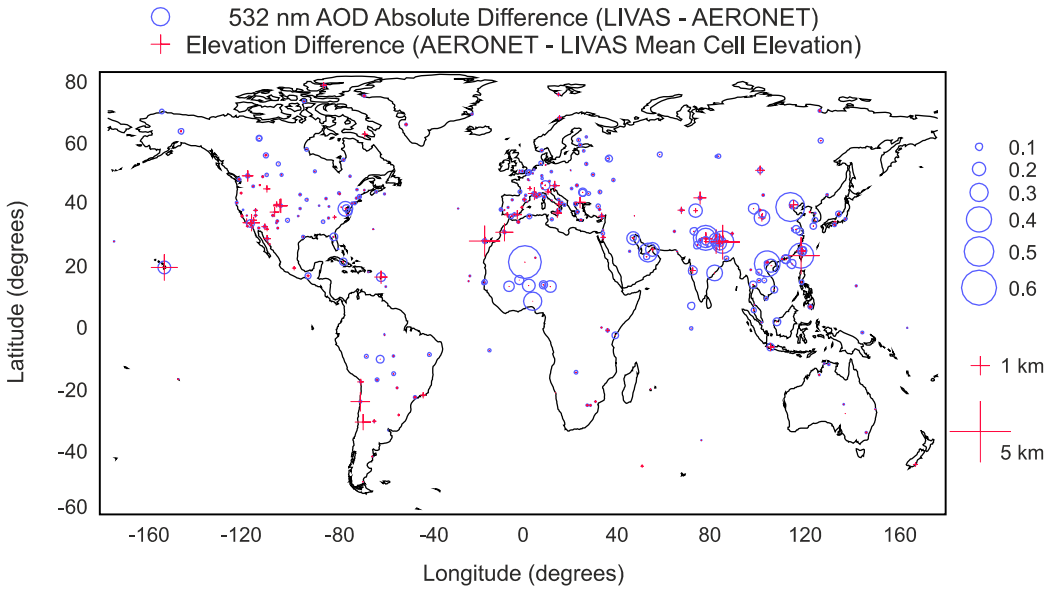


1

2 **Figure 12**

3

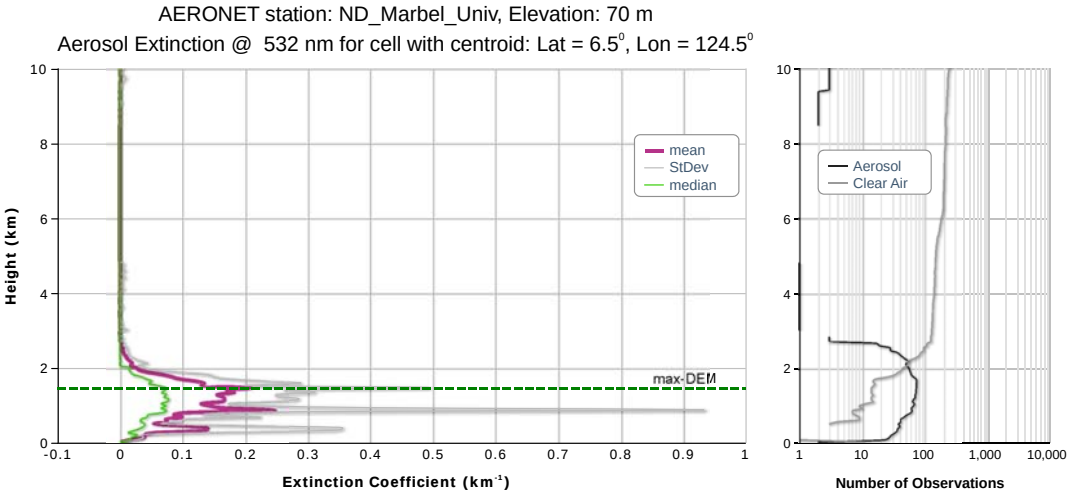
AERONET station: ND_Marbel_Univ, Elevation: 70 m
Aerosol Extinction @ 532 nm for cell with centroid: Lat = 6.5°, Lon = 124.5°
Height (km)
Extinction Coefficient (km-1)
mean
StDev
median
max-DEM
Aerosol
Clear Air
Number of Observations

**Figure 13**

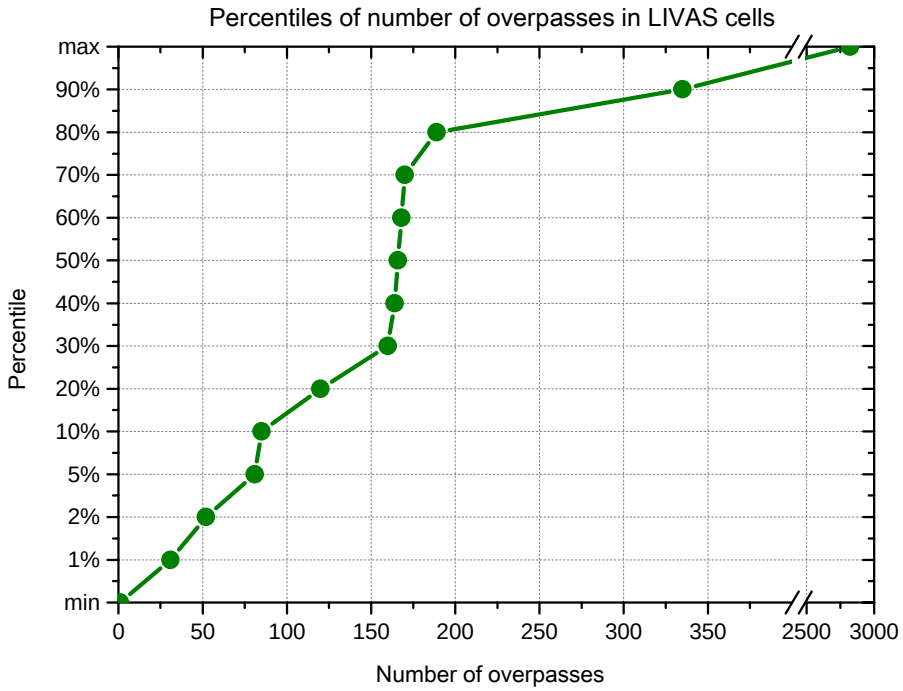
Percentiles of number of overpasses in LIVAS cells
Percentile
max
90%
80%
70%
60%
50%
40%
30%
20%
10%
5%
2%
1%
min
0
50
100
150
200
250
300
350
2500
3000
Number of overpasses

**Figure 14**

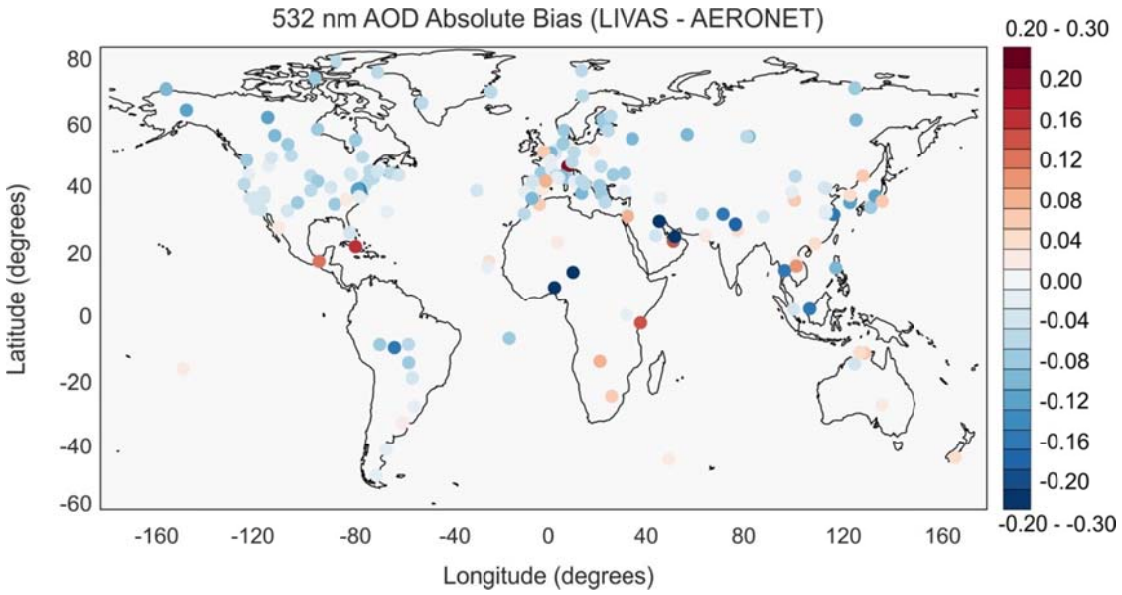
532 nm AOD Absolute Bias (LIVAS - AERONET)
Latitude (degrees)
80
60
40
20
0
-20
-40
-60
-160
-120
-80
-40
0
40
80
120
160
Longitude (degrees)
0.20 - 0.30
0.20
0.16
0.12
0.08
0.04
0.00
-0.04
-0.08
-0.12
-0.16
-0.20
-0.20 - -0.30

**Figure 15**

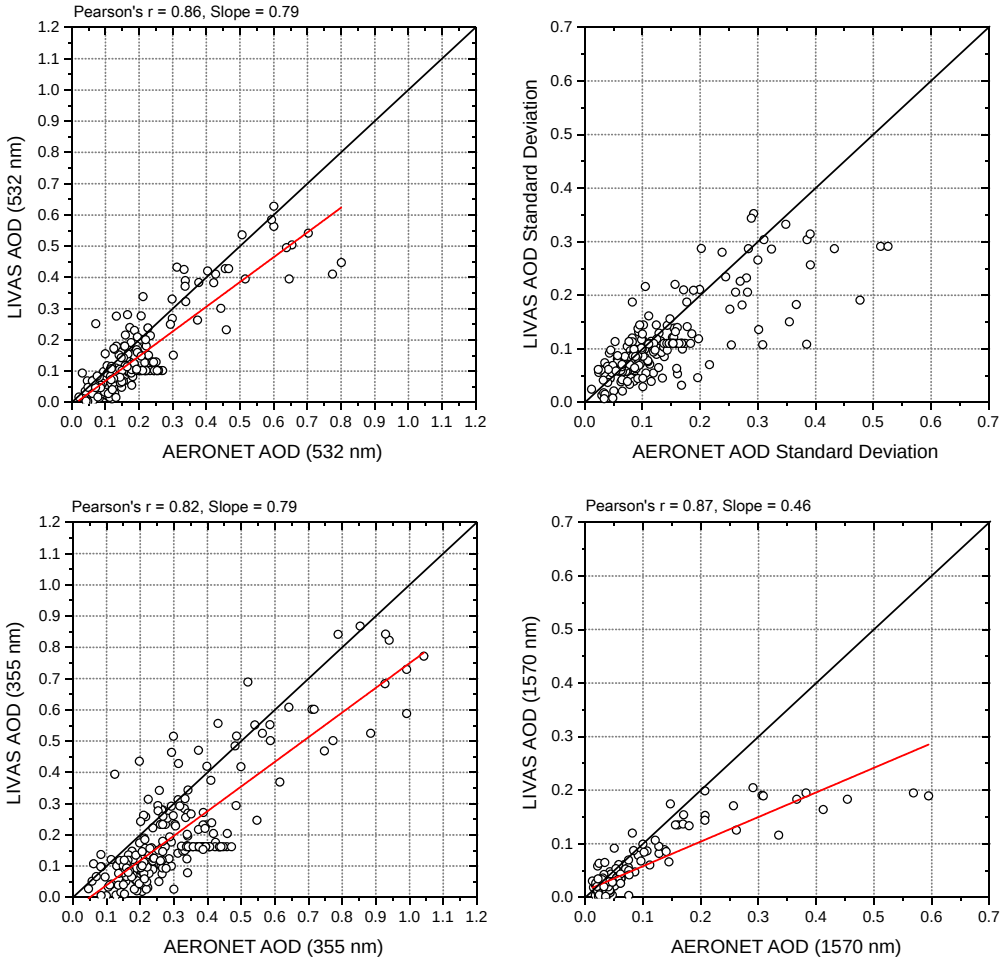
Pearson's r = 0.86, Slope = 0.79
LIVAS AOD (532 nm)
AERONET AOD (532 nm)
LIVAS AOD Standard Deviation
AERONET AOD Standard Deviation
Pearson's r = 0.82, Slope = 0.79
LIVAS AOD (355 nm)
AERONET AOD (355 nm)
Pearson's r = 0.87, Slope = 0.46
LIVAS AOD (1570 nm)
AERONET AOD (1570 nm)

**Figure 16**

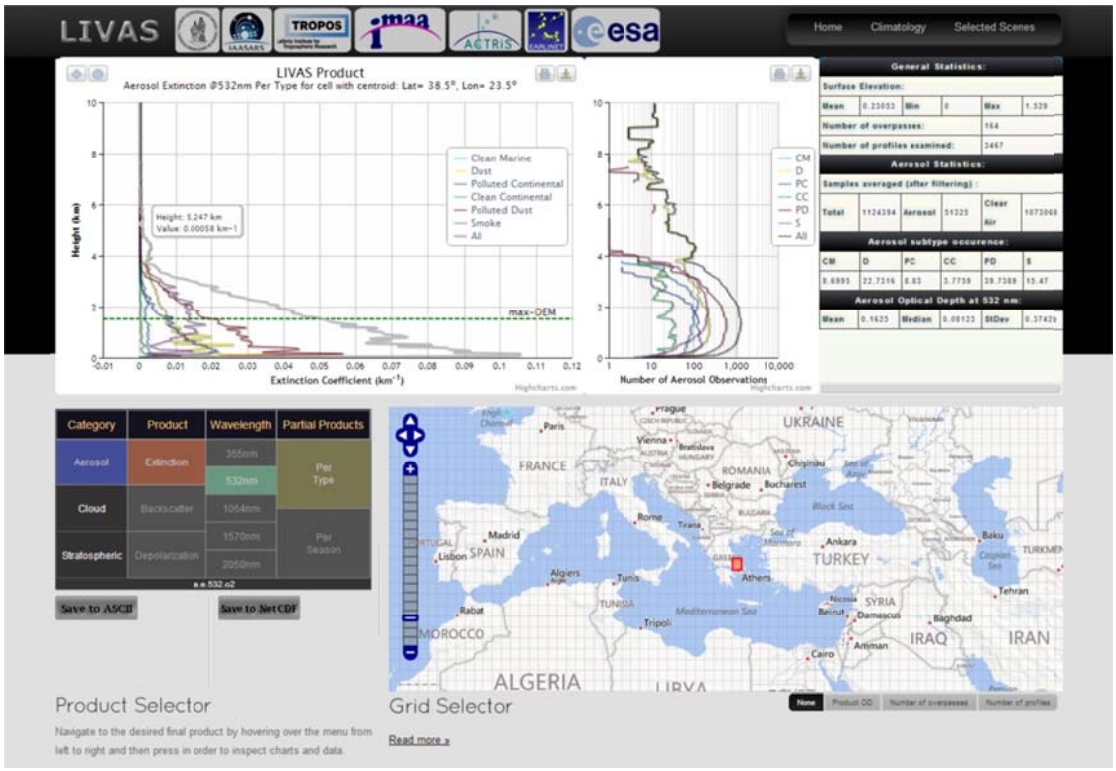
LIVAS
TROPOS
Home
Climatology
Selected Scenes
LIVAS Product
Aerosol Extincton @532nm Per Type for cell with centroid: Lat= 38.5°, Lon= 23.5°
Clean Marine
Dust
Polluted Continental
Clean Continental
Polluted Dust
Smoke
All
max-DEM
Extinction Coefficient (km⁻¹)
Number of Aerosol Observations
General Statistics:
Aerosol Statistics:
Aerosol subtype occurence:
Aerosol Optical Depth at 532 nm:
Category
Product
Wavelength
Partial Products
Aerosol
Extinction
Cloud
Backscatter
Stratospheric
Depolarization
355nm
532nm
1064nm
1570nm
2050nm
Per Type
Per Season
Save to ASCII
Save to NetCDF
Product Selector
Navigate to the desired final product by hovering over the menu from left to right and then press in order to inspect charts and data.
Grid Selector
Read more »
UKRAINE
FRANCE
ITALY
ROMANIA
SPAIN
TURKEY
SYRIA
IRAQ
IRAN
MOROCCO
ALGERIA
Paris
Vienna
Belgrade
Bucharest
Rome
Madrid
Lisbon
Athens
Ankara
Tehran
Baghdad
Cairo
Amman
Damascus
Tripoli
Tunis
Algiers
Rabat

**Figure 17**

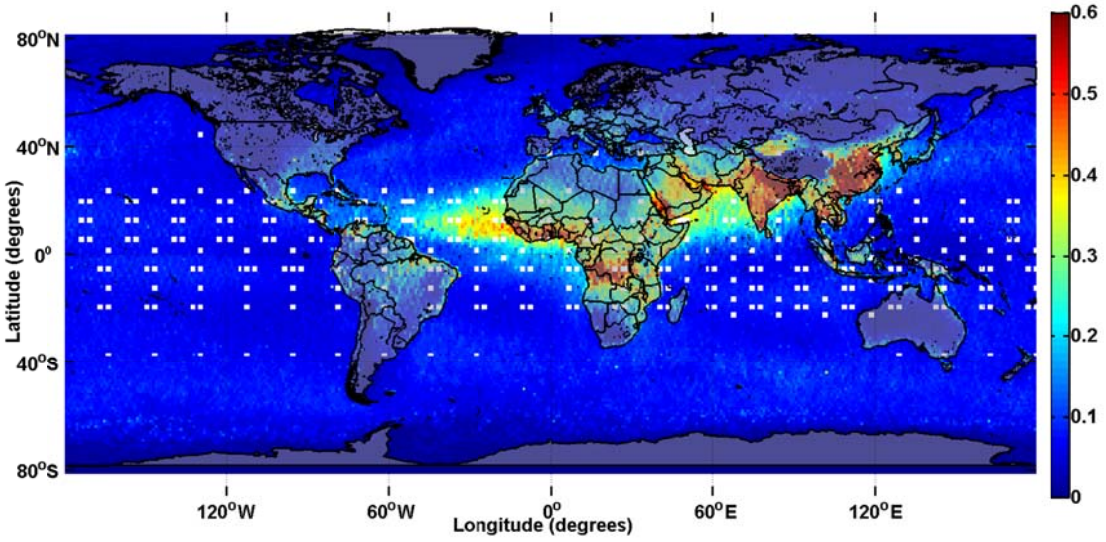
80°N
40°N
0°
40°S
80°S
Latitude (degrees)
120°W
60°W
0°
60°E
120°E
Longitude (degrees)
0.6
0.5
0.4
0.3
0.2
0.1
0

**Figure 18**

## REFERENCES


Amiridis, V., Wandinger, U., Marinou, E., Giannakaki, E., Tsekeri, A., Basart, S., Kazadzis, S., Gkikas, A., Taylor, M., Baldasano, J., and Ansmann, A., Optimizing CALIPSO Saharan dust retrievals, Atmos. Chem. Phys., 13, 12089-12106, doi:10.5194/acp-13-12089-2013, 2013.

Böckmann C., et al., Aerosol lidar intercomparison in the framework of the EARLINET project. 2. Aerosol backscatter algorithms, Appl. Opt. 43, 977-989, 2004.

Bösenberg, J., Matthias, V., Amodeo, A., Amiridis, V., Ansmann, A., et al., EARLINET: A European Aerosol Research Lidar Network to Establish an Aerosol Climatology, Max-Planck-Institut Report No. 348, 2003.

Burton, S. P., Ferrare, R. A., Vaughan, M. A., Omar, A. H., Rogers, R. R., Hostetler, C. A., and Hair, J. W., Aerosol classification from airborne HSRL and comparisons with the CALIPSO vertical feature mask, Atmos. Meas. Tech., 6, 1397-1412, doi:10.5194/amt-6-1397-2013, 2013.

Campbell, J. R., Reid, J. S., Westphal, D. L., Zhang, J., Tackett, J. L., Chew, B. N., Welton, E. J., Shimizu, A., Sugimoto, N., Aoki, K., and Winker, D. M., Characterizing the vertical profile of aerosol particle extinction and linear depolarization over Southeast Asia and the Maritime Continent: the 2007–2009 view from CALIOP, Atmos. Res., doi:10.1016/j.atmosres.2012.05.007, 2012.

Deshler, T., Johnson, B. J., & Rozier, W. R., Balloonborne measurements of Pinatubo aerosol during 1991 and 1992 at 41° N: vertical profiles, size distribution, and volatility. Geophys. Res. Lett. 20, 1435–1438, 1993.

Dubovik, O., and King, M. D., A flexible inversion algorithm for retrieval of aerosol optical properties from sun and sky radiance measurements, J. Geophys. Res., 105, 20,673–20,696, 2000.

Dubovik, O., Smirnov, A., Holben, B. N., King, M. D., et al., Accuracy assessments of aerosol optical properties retrieved from Aerosol Robotic Network (AERONET) Sun and sky radiance measurements, J. Geophys. Res., 105, 9791– 9806, 2000.

Dubovik, O., Sinyuk, A., Lapyonok, T., Holben, B. N., Mishchenko, M., Yang, P., Eck, T. F., Volten, H., Muñoz, O., Veihelmann, B., van der Zande, W. J., Leon, J.-F., Sorokin, M. and Slutsker, I.: Application of spheroid models to account for aerosol particle nonsphericity in remote sensing of desert dust, J. Geophys. Res., 111(D11), D11208, doi:10.1029/2005JD006619, 2006.ESA, Reports for Mission Selection, The Six Candidate Earth Explorer Missions, EarthCARE – Earth Clouds, Aerosols and Radiation Explorer, ESA-SP-1279(1), 2004.

Eck, T. F., Holben, B. N., Slutsker, I. and Setzer, A.: Measurements of irradiance attenuation and estimation of aerosol single scattering albedo for biomass burning aerosols in Amazonia, J. Geophys. Res. 103, 31865-31878, 1998.

Eck, T. F., Holben, B. N., Reid, J. S., Dubovik, O., Smirnov, A., O'Neill, N. T., Slutsker, I., and Kinne, S.: Wavelength dependence of the optical depth of biomass burning, urban, and desert dust aerosols, J. Geophys. Res., 104(D24), 31,333–31,349, 1999.

Eck, T. F., Holben, B. N., Reid, J. S., O'Neill, N. T., Schafer, J. S., Dubovik, O., Smirnov, A., Yamasoe, M. A. and Artaxo, P.: High aerosol optical depth biomass burning events: A comparison of optical properties for different source regions, Geophys. Res. Lett., 30, 2035, doi:10.1029/2003GL017861, 20, 2003.

Freudenthaler, V., et al., Depolarization ratio profiling at several wavelengths in pure Saharan dust during SAMUM 2006, Tellus, Ser. B, 61, 165–179, doi:10.1111/j.1600–0889.2008.00396.x., 2009.

Freudenthaler, V., et al., EARLI09 – direct intercomparison of eleven EARLINET lidar systems, in: Proceedings of the 25th International Laser Radar Conference, St. Petersburg, Russia, 5–9 July, 891–894, 2010.

Groß, S., Tesche, M., Freudenthaler, V., Toledano, C., Wiegner, M., Ansmann, A., Althausen, D. & Seefeldner, M., Characterization of Saharan dust, marine aerosols and a mixture of biomass burning aerosols and dust by means of multiwavelength depolarization and Raman measurements during SAMUM-2, Tellus, Ser. B, 63, 706–724. doi: 10.1111/j.1600-0889.2011.00556.x, 2011a.

Groß, S., et al., Dual-wavelength linear depolarization ratio of volcanic aerosols: Lidar measurements of the Eyjafjallajökull plume over Maisach, Germany, Atmospheric Environment, doi:10.1016/j.atmosenv.2011.06.017, 2011b.

Hasekamp, O., Litvinov, P., and Butz, A.: Aerosol properties over the ocean from PARASOL multi-angle photopolarimetric measurements, J. Geophys. Res., 116, D14204, doi:10.1029/2010JD015469, 2011.

Hess, M., Köpke, P. & Schult, I., Optical properties of aerosols and clouds: the software package OPAC. Bull. Am. Meteorol. Soc. 79, 831–844, 1998.

Holben, B. N., Eck, T. F., Slutsker, I., Tanre, D., Buis, J. P., Setzer, A., Vermote, E., Reagan, J. A., Kaufman, Y. J. and Nakajima, T.: AERONET—A federated instrument network and data archive for aerosol characterization, Remote sensing of environment, 66(1), 1–16, 1998.

Holben, B. N., Tanré, D., Smirnov, A., Eck, T. F., Slutsker, I., Abuhassan, N., Newcomb, W. W., Schafer, J. S., Chatenet, B., Lavenu, F., Kaufman, Y. J., Vande Castle, J., Setzer, A., Markham, B., Clark, D., Frouin, R., Halthore, R., Karneli, A., O'Neill, N. T., Pietras, C., Pinker, R. T., Voss, K., and Zibordi, G.: An emerging ground-based aerosol climatology: Aerosol optical depth from AERONET, Journal of Geophysical Research D: Atmospheres, 106(D11), 12067-12097, doi:10.1029/2001JD900014, 2001.

Holler, R., Ito, K., Tohno, S., and Kasahara, M.: Wavelengthdependent aerosol single-scattering albedo: Measurements and model calculations for a coastal site near the Sea of Japan during ACE-Asia, J. Geophys. Res., 108(D23), 8648, doi:10.1029/2002JD003250, 2003.

Illingworth, A., Barker, H., Beljaars, A., Ceccaldi, M., Chepfer, H., Colec, J., Delanoe, J., Domenech, C., Donovan, D., Fukuda, S., Hirakata, M., Hogan, R., Huenerbein, A., Kollias, P., Kubota, T., Nakajima, T., Nakajima, T., Nishizawa, T., Ohno, Y., Okamoto, H., Oki, R., Sato, K., Satoh, M., Shephard, M., Wandinger, U., Wehr, T., Zadelhoff, G-J., The EARTHCARE satellite: the next step forward in global measurements of clouds, aerosols, precipitation and radiation, BAMS-D-12-00227, 2014 (in print).

Jung, J., Kim, Y. J., Lee, K. Y., -Cayetano, M. G., Batmunkh, T., Koo, J.-H., and Kim, J.: Spectral optical properties of long-range transport Asian dust and pollution aerosols over Northeast Asia in 2007 and 2008, Atmos. Chem. Phys., 10, 5391-5408, doi:10.5194/acp-10-5391-2010, 2010.

Kanitz, T., Ansmann, A., Foth, A., Seifert, P., Wandinger, U., Engelmann, R., Baars, H., Althausen, D., Casiccia, C., and Zamorano, F., Surface matters: limitations of CALIPSO V3 aerosol typing in coastal regions, Atmos. Meas. Tech. Discuss., 7, 1333-1365, doi:10.5194/amtd-7-1333-2014, 2014.

Kim, S.-W., Yoon, S.-C., Kim, J., and Kim, S.-Y.: Seasonal and monthly variations of columnar aerosol optical properties over East Asia determined from multi-year MODIS, LIDAR, and AERONET Sun/sky radiometer measurements, Atmos. Environ., 41, 1634–1651, 2007.

Liu, Z., Vaughan, M., Winker, D., Kittaka, C., Getzewich, B., Kuehn, R., Omar, A., Powell, K., Trepte, C., and Hostetler, C.: The CALIPSO Lidar Cloud and Aerosol Discrimination: Version 2 Algorithm and Initial Assessment of Performance. J. Atmos. Oceanic Technol., 26, 1198–1213, doi:10.1175/2009jtecha1229.1, 2009.

Mamouri, R. E., Ansmann, A., Nisantzi, A., Kokkalis, P., Schwarz, A., and Hadjimitsis, D.: Low Arabian dust extinction-to-backscatter ratio, Geophys. Res. Lett., 40, doi:10.1002/grl.50898, 2013.

Matthias V., et al., Aerosol lidar inter-comparison in the framework of the EARLINET project. 1 Instruments, Appl. Opt., 43, N. 4, 961-976, 2004.

McConnell, C. L., Highwood, E. J., Coe, H., Formenti, P., Anderson, B., Osborne, S., Nava, S., Desboeufs, K., Chen, G., and Harrison, M. A. J.: Seasonal variations of the physical and optical characteristics of Saharan dust: Results from the Dust Outflow and Deposition to the Ocean (DODO) experiment, J. Geophys. Res., 113, D14S05, doi:10.1029/2007JD009606, 2008.

Mie, G., Beiträge zur Optik trüber Medien, speziell kolloidaler Metallösungen, Ann. Phys., 25(4), 377–445, 1908.

Mishchenko, M. I., Travis, L. D., and Lacis, A. A., Scattering, Absorption, and Emission of Light by Small Particles, Cambridge Univ. Press, New York, 2002. (Available at http://www.giss.nasa.gov/~crmim/books.html)

Mueller, D., A. Ansmann, I. Mattis, M. Tesche, U. Wandinger, D. Althausen, and G. Pisani, Aerosol-type-dependent lidar ratios observed with Raman lidar, J. Geophys. Res., 112, D16202, doi:10.1029/2006JD008292, 2007.

Müller, T., Schladitz, A., Massling, A., Kaaden, N., Wiedensohler, A., Kandler, K.: Spectral absorption coefficients and imaginary parts of refractive indices of Saharan dust during SAMUM-1. Tellus, 61B, 79-95, 2011.

Omar, A. H., Winker, D. M., Kittaka, C., Vaughan, M. A., Liu, Z. Y., Hu, Y. X., Trepte, C. R., 20 Rogers, R. R., Ferrare, R. A., Lee, K. P., Kuehn, R. E., and Hostetler, C. A.: The CALIPSO automated aerosol classification and lidar ratio selection algorithm, J. Atmos. Ocean. Tech., 26, 1994–2014, doi:10.1175/2009jtecha1231.1, 2009.

O'Neill, N. T., Eck, T. F., Smirnov, A., Holben, B. N. and Thulasiraman, S.: Spectral discrimination of coarse and fine mode optical depth, Journal of Geophysical Research, 108(D17), 4559, 2003.

Omar, A. H., Winker, D. M., Tackett, J. L., Giles, D. M., Kar, J., Liu, Z., Vaughan, M. A., Powell, K. A., and Trepte, C. R.: CALIOP and AERONET aerosol optical depth comparisons: One size fits none, J. Geophys. Res. Atmos., 118, 4748–4766, doi:10.1002/jgrd.50330, 2013.

Omar, A. H., Won, J.-G., Winker, D. M., Yoon, S.-C., Dubovik, O. & Mc- Cormick, M. P., Development of global aerosol models using cluster analysis of Aerosol Robotic Network (AERONET) measurements, J. Geophys. Res., 110, doi: 10.1029/2004JD004874. 177, 2005.

Pappalardo, G., A. Amodeo, M. Pandolfi, U. Wandinger, A. Ansmann, J. Bosenberg, V. Matthias, V. Amiridis, F. De Tomasi, M. Frioud, M. Iarlori, L. Komguem, A. Papayannis, F. Rocadenbosch, and X. Wang, Aerosol lidar intercomparison in the

framework of the EARLINET project. 3. Raman lidar algorithm for aerosol extinction, backscatter and lidar ratio, Appl. Opt., 43. N. 28, 5370-5385, 2004.

Pappalardo, G., Wandinger, U., Mona, L., Hiebsch, A., Mattis, I., Amodeo, A., Ansmann, A., Seifert, P., Linne, H., Apituley, 5 A., Alados Arboledas, L., Balis, D., Chaikovsky, A., D'Amico, G., De Tomasi, F., Freudenthaler, V., Giannakaki, E., Giunta, A., Grigorov, I., Iarlori, M., Madonna, F., Mamouri, R.-E., Nasti, L., Papayannis, A., Pietruczuk, A., Pujadas, M., Rizi, V., Rocadenbosch, F., Russo, F., Schnell, F., Spinelli, N., Wang, X., and Wiegner, M.: EARLINET correlative measurements for CALIPSO: first intercomparison results, J. Geophys. Res., 115, D00H19, doi:10.1029/2009JD012147, 2010.

Pappalardo, G., Amodeo, A., Apituley, A., Comeron, A., Freudenthaler, V., Linné, H., Ansmann, A., Bösenberg, J., D'Amico, G., Mattis, I., Mona, L., Wandinger, U., Amiridis, V., Alados-Arboledas, L., Nicolae, D., and Wiegner, M.: EARLINET: towards an advanced sustainable European aerosol lidar network, Atmos. Meas. Tech. Discuss., 7, 2929-2980, doi:10.5194/amtd-7-2929-2014, 2014.

Reid, J. S., Koppmann, R., Eck, T. F., and Eleuterio, D. P.: A review of biomass burning emissions part II: intensive physical properties of biomass burning particles, Atmos. Chem. Phys., 5, 799-825, doi:10.5194/acp-5-799-2005, 2005.

Sayer, A. M., A. Smirnov, N. C. Hsu, and B. N. Holben, A pure marine aerosol model, for use in remote sensing applications, J. Geophys. Res., 117, D05213, doi:10.1029/2011JD016689, 2012.

Schuster, G. L., Vaughan, M., MacDonnell, D., Su, W., Winker, D., Dubovik, O., Lapyonok, T., and Trepte, C.: Comparison of CALIPSO aerosol optical depth retrievals to AERONET measurements, and a climatology for the lidar ratio of dust, Atmos. Chem. Phys., 12 (16), 7431-7452, doi:10.5194/acp-12-7431-2012, 2012.

Smirnov, A., Holben, B. N., Kaufman, Y. J., Dubovik, O., Eck, T. F., Slutsker, I., Pietras, C., and Halthore, R. N.: Optical properties of atmospheric aerosol in maritime environments.J. Atmos. Sci., 59, 501–523, 2002.

Stoffelen, A., et al., The Atmospheric Dynamics Mission for Global Wind Field Measurements, BAMS, 86 (1), 73-87, 2005.

Tesche, M., Wandinger, U., Ansmann, A., Althausen, D., Müller, D., and Omar, A.H.: Ground-based validation of CALIPSO observations of dust and smoke in the Cape Verde region, Journal of Geophysical Research, Vol. 118, 1–14, doi:10.1002/jgrd.50248, 2013.

The EARLINET publishing group 2000–2010: Adam, M., Alados-Arboledas, L., Althausen, D., Amiridis, V., Amodeo, A., Ansmann, A., Apituley, A., Arshinov, Y., Balis, D., Belegante, L., Bobrovnikov, S., Boselli, A., Bravo-Aranda, J. A., Bösenberg, J., Carstea, E., Chaikovsky, A., Comerón, A., D'Amico, G., Daou, D., Dreischuh, T., Engelmann, R., Finger, F., Freudenthaler, V., Garcia-Vizcaino, D., García, A. J. F., Geiß, A., Giannakaki, E., Giehl, H., Giunta, A., de Graaf, M., Granados-Muñoz, M. J., Grein, M., Grigorov, I., Groß, S., Gruening, C., Guerrero-Rascado, J. L., Haeffelin, M., Hayek, T., Iarlori, M., Kanitz, T., Kokkalis, P., Linné, H., Madonna, F., Mamouriat, R.-E., Matthias, V., Mattis, I., Menéndez, F. M., Mitev, V., Mona, L., Morille, Y., Muñoz, C., Müller, A., Müller, D., Navas-Guzmán, F., Nemuc, A., Nicolae, D., Pandolfi, M., Papayannis, A., Pappalardo, G., Pelon, J., Perrone, M. R., Pietruczuk, A., Pisani, G., Potma, C., Preißler, J., Pujadas, M., Putaud, J., Radu, C., Ravetta, F., Reigert, A., Rizi, V., Rocadenbosch, F., Rodríguez, A., Sauvage, L., Schmidt, J., Schnell, F., Schwarz, A., Seifert, P., Serikov, I., Sicard, M., Silva, A. M., Simeonov, V., Siomos, N., Sirch, T., Spinelli, N., Stoyanov, D., Talianu, C., Tesche, M., De Tomasi, F., Trickl, T., Vaughan, G., Volten, H., Wagner, F., Wandinger, U., Wang, X., Wiegner, M., and Wilson, K. M.: EARLINET all observations (2000–2010), World Data Center for Climate (WDCC), doi:10.1594/WDCC/EN_all_measurements_2000-2010, 2014a.

The EARLINET publishing group 2000–2010: Adam, M., Alados-Arboledas, L., Althausen, D., Amiridis, V., Amodeo, A., Ansmann, A., Apituley, A., Arshinov, Y., Balis, D., Belegante, L., Bobrovnikov, S., Boselli, A., Bravo-Aranda, J. A., Bösenberg, J., Carstea, E., Chaikovsky, A., Comerón, A., D'Amico, G., Daou, D., Dreischuh, T., Engelmann, R., Finger, F., Freudenthaler, V., Garcia-Vizcaino, D., García, A. J. F., Geiß, A., Giannakaki, E., Giehl, H., Giunta, A., de Graaf, M., Granados-Muñoz, M. J., Grein, M., Grigorov, I., Groß, S., Gruening, C., Guerrero-Rascado,

J. L., Haeffelin, M., Hayek, T., Iarlori, M., Kanitz, T., Kokkalis, P., Linné, H., Madonna, F., Mamouriat, R.E., Matthias, V., Mattis, I., Menéndez, F. M., Mitev, V., Mona, L., Morille, Y., Muñoz, C., Müller, A., Müller, D., Navas-Guzmán, F., Nemuc, A., Nicolae, D., Pandolfi, M., Papayannis, A., Pappalardo, G., Pelon, J., Perrone, M.R., Pietruczuk, A., Pisani, G., Potma, C., Preißler, J., Pujadas, M., Putaud, J., Radu, C., Ravetta, F., Reigert, A., Rizi, V., Rocadenbosch, F., Rodríguez, A., Sauvage, L., Schmidt, J., Schnell, F., Schwarz, A., Seifert, P., Serikov, I., Sicard, M., Silva, A. M., Simeonov, V., Siomos, N., Sirch, T., Spinelli, N., Stoyanov, D., Talianu, C., Tesche, M., De Tomasi, F., Trickl, T., Vaughan, G., Volten, H., Wagner, F., Wandinger, U., Wang, X., Wiegner, M., and Wilson, K. M.: EARLINET climatology (2000–2010), World Data Center for Climate (WDCC), doi:10.1594/WDCC/EN_Climatology_2000-2010, 2014b.

The EARLINET publishing group 2000–2010: Adam, M., Alados-Arboledas, L., Althausen, D., Amiridis, V., Amodeo, A., Ansmann, A., Apituley, A., Arshinov, Y., Balis, D., Belegante, L., Bobrovnikov, S., Boselli, A., Bravo-Aranda, J. A., Bösenberg, J., Carstea, E., Chaikovsky, A., Comerón, A., D'Amico, G., Daou, D., Dreischuh, T., Engelmann, R., Finger, F., Freudenthaler, V., Garcia-Vizcaino, D., García, A. J. F., Geiß, A., Giannakaki, E., Giehl, H., Giunta, A., de Graaf, M., Granados-Muñoz, M. J., Grein, M., Grigorov, I., Groß, S., Gruening, C., Guerrero-Rascado, J. L., Haeffelin, M., Hayek, T., Iarlori, M., Kanitz, T., Kokkalis, P., Linné, H., Madonna, F., Mamouriat, R.-E., Matthias, V., Mattis, I., Menéndez, F. M., Mitev, V., Mona, L., Morille, Y., Muñoz, C., Müller, A., Müller, D., Navas-Guzmán, F., Nemuc, A., Nicolae, D., Pandolfi, M., Papayannis, A., Pappalardo, G., Pelon, J., Perrone, M. R., Pietruczuk, A., Pisani, G., Potma, C., Preißler, J., Pujadas, M., Putaud, J., Radu, C., Ravetta, F., Reigert, A., Rizi, V., Rocadenbosch, F., Rodríguez, A., Sauvage, L., Schmidt, J., Schnell, F., Schwarz, A., Seifert, P., Serikov, I., Sicard, M., Silva, A. M., Simeonov, V., Siomos, N., Sirch, T., Spinelli, N., Stoyanov, D., Talianu, C., Tesche, M., De Tomasi, F., Trickl, T., Vaughan, G., Volten, H., Wagner, F., Wandinger, U., Wang, X., Wiegner, M., and Wilson, K. M.: EARLINET correlative observations for CALIPSO (2006–2010),World Data Center for Climate (WDCC), doi:10.1594/WDCC/EN_Calipso_2006-2010, 2014c.

The EARLINET publishing group 2000-2010, Adam, M., Alados-Arboledas, L., Althausen, D., Amiridis, V., Amodeo, A., Ansmann, A., Apituley, A., Arshinov, Y., Balis, D., Belegante, L., Bobrovnikov, S., Boselli, A., Bravo-Aranda, J. A., Bösenberg, J., Carstea, E., Chaikovsky, A., Comerón, A., D'Amico, G., Daou, D., Dreischuh, T., Engelmann, R., Finger, F., Freudenthaler, V., Garcia-Vizcaino, D., García, A. J. F., Geiß, A., Giannakaki, E., Giehl, H., Giunta, A., de Graaf, M., Granados-Muñoz, M. J., Grein, M., Grigorov, I., Groß, S., Gruening, C., Guerrero-Rascado, J. L., Haeffelin, M., Hayek, T., Iarlori, M., Kanitz, T., Kokkalis, P., Linné, H., Madonna, F., Mamouriat, R.-E., Matthias, V., Mattis, I., Menéndez, F. M., Mitev, V., Mona, L., Morille, Y., Muñoz, C., Müller, A., Müller, D., Navas-Guzmán, F., Nemuc, A., Nicolae, D., Pandolfi, M., Papayannis, A., Pappalardo, G., Pelon, J., Perrone, M. R., Pietruczuk, A., Pisani, G., Potma, C., Preißler, J., Pujadas, M., Putaud, J., Radu, C., Ravetta, F., Reigert, A., Rizi, V., Rocadenbosch, F., Rodríguez, A., Sauvage, L., Schmidt, J., Schnell, F., Schwarz, A., Seifert, P., Serikov, I., Sicard, M., Silva, A. M., Simeonov, V., Siomos, N., Sirch, T., Spinelli, N., Stoyanov, D., Talianu, C., Tesche, M., De Tomasi, F., Trickl, T., Vaughan, G., Volten, H., Wagner, F., Wandinger, U., Wang, X., Wiegner, M., and Wilson, K. M.: EARLINET observations related to volcanic eruptions (2000–2010), World Data Center for Climate (WDCC), doi:10.1594/WDCC/EN_VolcanicEruption_2000-2010, 2014d.

The EARLINET publishing group 2000–2010: Adam, M., Alados-Arboledas, L., Althausen, D., Amiridis, V., Amodeo, A., Ansmann, A., Apituley, A., Arshinov, Y., Balis, D., Belegante, L., Bobrovnikov, S., Boselli, A., Bravo-Aranda, J. A., Bösenberg, J., Carstea, E., Chaikovsky, A., Comerón, A., D'Amico, G., Daou, D., Dreischuh, T., Engelmann, R., Finger, F., Freudenthaler, V., Garcia-Vizcaino, D., García, A. J. F., Geiß, A., Giannakaki, E., Giehl, H., Giunta, A., de Graaf, M., Granados-Muñoz, M. J., Grein, M., Grigorov, I., Groß, S., Gruening, C., Guerrero-Rascado, J. L., Haeffelin, M., Hayek, T., Iarlori, M., Kanitz, T., Kokkalis, P., Linné, H., Madonna, F., Mamouriat, R.-E., Matthias, V., Mattis, I., Menéndez, F. M., Mitev, V., Mona, L., Morille, Y., Muñoz, C., Müller, A., Müller, D., Navas-Guzmán, F., Nemuc, A., Nicolae, D., Pandolfi, M., Papayannis, A., Pappalardo, G., Pelon, J., Perrone, M. R., Pietruczuk, A., Pisani, G., Potma, C., Preißler, J., Pujadas, M., Putaud, J., Radu, C., Ravetta, F., Reigert, A., Rizi, V., Rocadenbosch, F., Rodríguez, A., Sauvage, L., Schmidt, J., Schnell, F., Schwarz, A., Seifert, P., Serikov, I., Sicard, M., Silva, A. M.,

Simeonov, V., Siomos, N., Sirch, T., Spinelli, N., Stoyanov, D., Talianu, C., Tesche, M., De Tomasi, F., Trickl, T., Vaughan, G., Volten, H., Wagner, F., Wandinger, U., Wang, X., Wiegner, M., and Wilson, K. M.: EARLINET observations related to Saharan Dust events (2000–2010), World Data Center for Climate (WDCC), doi:10.1594/WDCC/EARLINET_SaharanDust_2000-2010, 2014e.Toledano, C., Wiegner, M., Gross, S., Freudenthaler, V., Gasteiger, J., Müller, D., Müller, T., Schladitz, A., Weinzierl, B., Torres B., and O'Neill, N. T.: Optical properties of aerosol mixtures derived from sun-sky radiometry during SAMUM-2. Tellus 63B, 635-648, doi: 10.1111/j.1600-0889.2011.00573.x, 2011.

Van de Hulst, H., Light Scattering by Small Particles, New York: Wiley, 1957.

Vaughan, J.M., Geddes, N.J., Flamant P.H., and Flesia C., Establishment of a backscatter coefficient and atmospheric database, DERA Report for ESA Contract no. 12510/97/NL/RE, DERA/EL/ISET/CR980139/1.0, 1998.

Vaughan, M. A., Powell, K. A., Kuehn, R. E., Young, S. A., Winker, D. M., Hostetler, C. A., Hunt, W. H., Liu, Z. Y., McGill, M. J., and Getzewich, B. J.: Fully automated detection of cloud and aerosol layers in the CALIPSO lidar measurements, J. Atmos. Ocean. Tech., 26, 2034–2050, doi:10.1175/2009jtecha1228.1, 2009.

Volten, H., O. Munoz, E. Rol, J. F. de Haan, W. Vassen, J. W. Hovenier, K. Muinonen, and T. Nousiainen: Scattering matrices of mineral aerosol particles at 441.6 nm and 632.8 nm, J. Geophys. Res., 106, 17, 375–17, 401, 2001.

Wandinger, U., Ansmann, A., Reichardt, J., Deshler, T., Determination of stratospheric aerosol microphysical properties from independent extinction and backscattering measurements with a Raman lidar, Appl Opt., 34(36), 8315-29. doi: 10.1364/AO.34.008315, 1995.

Wandinger, U., Tesche, M., Seifert, P., Ansmann, A., Müller, D., and Althausen, D.: Size matters: Influence of multiple scattering on CALIPSO light-extinction profiling in desert dust, Geophysical Research Letters, 37 (10), L10801, doi: 10.1029/2010GL042815, 2010.

Wandinger U., Hiebsch, A., Mattis, I., Pappalardo, G., Mona, L., and Madonna F., Aerosols and Clouds: Long-term Database from Spaceborne Lidar Measurements, Executive Summary, http://esamultimedia.esa.int/docs/gsp/C21487ExS.pdf, ESTEC Contract 21487/08/NL/HE, 2011.

Weinzierl, B., Petzold, A., Esselborn, M., Wirth, M., Rasp, K., Kandler, K., Schütz, L., Koepke P., and Fiebig, M.: Airborne measurements of dust layer properties, particle size distribution and mixing state of Saharan dust during SAMUM 2006. Tellus 61B, 96-117 doi: 10.1111/j.1600-0889.2008.00392.x, 2009.

Winker, D. M., Vaughan, M. A., Omar, A., Hu, Y., Powell, K. A., Liu, Z., Hunt, W. H., and Young, S. A.: Overview of the CALIPSO mission and CALIOP data processing algorithms, J. Atmos. Ocean. Tech., 26, 2310–2323, doi: 10.1175/2009JTECHA1281.1, 2009.

Winker, D. M., Tackett, J. L., Getzewich, B. J., Liu, Z., Vaughan, M. A., and Rogers, R. R.: The global 3-D distribution of tropospheric aerosols as characterized by CALIOP, Atmos. Chem. Phys., 13, 3345-3361, doi:10.5194/acp-13-3345-2013, 2013.

Yang, P., and K. N. Liou, Geometric-optics-integral-equation method for light scattering by nonspherical ice crystals, Appl. Opt., 35, 6568–6584, 1996.

Young, S.A., and Vaughan, M. A.: The retrieval of profiles of particulate extinction from cloud-aerosol lidar infrared pathfinder satellite observations (CALIPSO) data: Algorithm description, Journal of Atmospheric and Oceanic Technology, 26 (6), pp. 1105-1119, doi: 10.1175/2008JTECHA1221.1, 2009.